

Anelastic and Electromechanical Properties of Doped and Reduced Ceria

Ellen Wachtel, Anatoly I. Frenkel, and Igor Lubomirsky*

Room-temperature mechanical properties of thin films and ceramics of doped and undoped ceria are reviewed with an emphasis on the anelastic behavior of the material. Notably, the unrelaxed Young's modulus of Gd-doped ceria ceramics measured by ultrasonic pulse-echo techniques is >200 GPa, while the relaxed biaxial modulus, calculated from the stress/strain ratio of thin films, is ≈ 10 times smaller. Oxygen-deficient ceria exhibits a number of anelastic effects, such as hysteresis of the lattice parameter, strain-dependent Poisson's ratio, room-temperature creep, and nonclassical electrostriction. Methods of measuring these properties are discussed, as well as the applicability of Raman spectroscopy for evaluating strain in thin films of Gd-doped ceria. Special attention is paid to detection of the time dependence of anelastic effects. Both the practical advantages and disadvantages of anelasticity on the design and stability of microscopic devices dependent on ceria thin films are discussed, and methods of mitigating the latter are suggested, with the aim of providing a cautionary note for materials scientists and engineers designing devices containing thin films or bulk ceria, as well as providing data-based constraints for theoreticians who are involved in modeling of the unusual electrical and electromechanical properties of undoped and doped ceria.

1. Introduction: Point Defects and the Elasticity of Ceria


Thin films and ceramics of undoped and doped ceria have been the subject of many studies and review articles in the materials science literature. This persistent interest is due, at least in part, to the broad versatility of ceria in industrial applications: devices that require high levels of oxygen ion conductivity, e.g., fuel cells and sensors^[1–3] as well as catalytic converters benefiting from the redox properties of the Ce ion.^[4,5] In the past, reviews have generally focused on the conductivity or catalytic

activity of ceria: the temporal, thermal, and compositional influence on the material elasticity was little examined. However, during the last decade, considerable interest has developed in doped ceria as an essential component in micrometer-sized fuel cells,^[6] sensors, and even electromechanical actuators.^[7] These scaled-down devices demand particularly precise mechanical engineering, e.g., because thermal cycling of ceria films during device operation can be associated with the generation of unpredictable mechanical strain. To give an example, the linear thermal expansion coefficient of undoped ceria is $\approx 11 \times 10^{-6} \text{ K}^{-1}$, which predicts that heating from 300 to 500 K will generate strain 0.22%. The fractional linear expansion of silicon within the same temperature range is only 0.063%; and therefore, heating a ceria film deposited on a silicon substrate would produce in-plane compressive strain in the film of 0.16%. Taking into account that the literature value for the elastic (Young's) modulus of undoped ceria is $\approx 200\text{--}300 \text{ GPa}$ ^[8–11] and that Poisson's ratio is 0.28, a thin film of ceria should develop in-plane compressive stress $\approx 430 \text{ MPa}$. A ceria film with thickness on the order of a few hundred nanometers cannot sustain such stress: the elastic energy stored exceeds typical adhesion energy. Therefore, the film would be expected to delaminate from the substrate, i.e., blister. However, delamination is not observed; and as discussed below, there is evidence from measurements of the substrate curvature that, following thermal cycling, the anelastic properties of oxygen-deficient ceria appear to reduce the relaxed biaxial Young's modulus of the substrate-supported films to much lower values.

Point defects in solids can give rise to anelastic behavior—i.e., the material completely recovers from deformation due to anisotropic application of stress, but with variable rates of strain release—provided that the defects behave as elastic dipoles, producing an anisotropic, local distortion of the crystal lattice. When thin films of ceria experience substrate clamping, only in-plane stress components are present. The in-plane strain is fully recoverable if and when the substrate is removed. Similarly, if ceramics are subjected to arbitrary mechanical loading (not necessarily isostatic), lattice deformation is fully recoverable, unless loading is performed at very high temperatures (above 1000 °C) when dislocation movement and grain boundary creep induce plastic (irrecoverable) deformation.

Dr. E. Wachtel, Prof. I. Lubomirsky
Department of Materials and Interfaces
Weizmann Institute of Science
Rehovot, Israel
E-mail: Igor.Lubomirsky@weizmann.ac.il

Prof. A. I. Frenkel
Department of Materials Science and Chemical Engineering
Stony Brook University
NY, USA

 The ORCID identification number(s) for the author(s) of this article can be found under <https://doi.org/10.1002/adma.201707455>.

DOI: 10.1002/adma.201707455

Introduction of a dopant ion produces local distortion of the lattice, which is present even in the absence of external stress. Since the lattice constant determined by XRD is actually an average of the total irradiated volume of the sample, the presence of dopants imposes an overall change in the lattice parameter, which may be viewed as isostatic strain. This isostatic strain is not accompanied by mechanical stress, and therefore does not modify mechanical response. On the other hand, local distortions have been viewed as the structural origin of the elastic dipoles, leading to the observed anelastic response to anisotropic stress. Consequently, no competition exists between these two factors: isostatic strain and substrate-induced compressive in-plane strain.

The anisotropic application of elastic stress, as, for example, in mechanical oscillations, leads to thermally activated reorientation of the elastic dipoles.^[12] However, when the applied stress is isotropic or hydrostatic, then no change in the elastic dipolar strain fields would be expected and a time-dependent relaxation process should not occur. In industrially useful forms of ceria, point defects include oxygen vacancies and dopant atoms substituting for the host at cation positions and they can occupy a significant fraction of the lattice sites. The fluorite crystal lattice (*Fm-3m*) is tolerant toward ion substitution; therefore, ceria is able to accommodate a relatively large concentration of dopants. For instance, in a frequently studied doped ceria composition, $\text{Ce}_{0.8}\text{Gd}_{0.2}\text{O}_{1.9}$, 20% of Ce ions are replaced by the aliovalent dopant (Gd^{3+}) and 5% of the oxygen sites are vacant. We note that a number of acronyms for the material composition may be found in the literature, e.g., Gd-doped ceria is referred to as $x\text{CGO}$, CGO_x , or $x\text{GDC}$ (used here), where x is the molar fraction of Gd. In undoped ceria, facile loss of oxygen and Ce redox reactions ($\text{Ce}^{4+} \leftrightarrow \text{Ce}^{3+}$) can produce additional complicating factors related to interaction between point defects. Nonstoichiometric, reduced ceria CeO_{2-x} presents a rich phase diagram at temperatures between ambient and 700 K and as a function of oxygen partial pressure.^[13,14] In a number of these crystal phases, neutron diffraction and reverse Monte Carlo modeling have shown that the oxygen vacancies preferentially align as pairs along the $\langle 111 \rangle$ direction rather than being randomly distributed among the anion sites.^[14] In Gd-, Sm-, or Nd-doped ceria, onset of oxygen vacancy ordering occurs when the aliovalent dopant concentration requires (for charge compensation) that ≥ 6 –10% of the oxygen sites are vacant,^[15–17] resulting in a change from *Fm-3m* to the double fluorite lattice (*Ia-3*).

Thus, point defects on the anion and cation sublattices of ceria can result in thermal and mechanical properties that are both difficult to characterize experimentally and also to model. Although the most striking of these properties may be attributed to the anelasticity of the material, quantitatively describing the particular sources of the anelastic behavior of ceria is beyond the scope of this review. The early, insightful book-length treatise on this topic by Nowick and Berry,^[12] "Anelastic Relaxation in Crystalline Solids," has provided the initial foundation for our approach. In spite of these difficulties, materials with a large concentration of point defects, interstitial as well as those located on lattice sites, are becoming of increasing practical interest. Responding to this challenge for the broad materials science community, we present a critical review of the results of measurement protocols suited to the elastic properties of undoped



Ellen Wachtel received her Ph.D. degree in applied physics from Yale University in 1970, and since 1976 has been a member of the Faculty of Chemistry of the Weizmann Institute of Science in Rehovot, Israel. Until her retirement in 2009, she was the head of the X-Ray Diffraction Laboratory, studying the structure of powders, fibers, and dispersions of both organic and inorganic materials. Currently, she is a consultant in the Department of Materials and Interfaces.



Anatoly I. Frenkel is a professor in the Department of Materials Science and Chemical Engineering, Stony Brook University, USA. He received his M.Sc. in physics from St. Petersburg University, Russia, and his Ph.D. degree in physics from Tel Aviv University. He studies the physicochemical properties of nanomaterials and the mechanisms of work of nanocatalysts, and develops operando methods of characterization using synchrotron X-ray techniques. He is a founding Principal Investigator and the Spokesperson of the Synchrotron Catalysis Consortium at Brookhaven National Laboratory.



Igor Lubomirsky is a professor in the Department of Materials and Interfaces, Weizmann Institute of Science (WIS), Israel. He obtained his B.Sc. in chemical engineering at Kharkov Polytechnic Institute (Ukraine) and his Ph.D. degree in solid-state chemistry at WIS. He held postdoctoral positions in electrical engineering at UCLA and the Max Planck Institute for Solid State Research (Stuttgart, Germany). His studies involve local symmetry reduction leading to anelastic and electrostrictive effects in solids with a large concentration of point defects, in general, and in ion conductors in particular.

and Gd-doped ceria ceramics and thin films, self-supported as well as substrate supported, under ambient conditions and at temperatures a few hundred degrees centigrade above ambient.

These techniques include impulse excitation technique (IET), nanoindentation, ultrasound pulse echo, Raman spectroscopy, and X-ray diffraction. How the mechanical properties of ceria may be related to the unanticipated electrostrictive activity is also discussed. Although providing the necessary constraints for atomic level modeling of the mechanical and electromechanical properties of ceria has been a subject of investigation by synchrotron X-ray diffraction, X-ray absorption spectroscopy, and neutron diffraction, the number of such structural studies currently exceeds 100 and correlating these findings with the observable mechanical properties and with each other obviously requires more detailed consideration than can be accommodated here.

2. Elastic Anomalies of Doped and Reduced Ceria

2.1. Measuring the Elastic Moduli of Anelastic Solids

An anelastic solid is a thermodynamic solid (unlike plastic or viscoelastic solids, which are not), although unlike elastic materials, once the applied stress (thermal or mechanical) is removed, relaxation to the initial state is not immediate. Anelastic effects in doped ceria have a number of similarities to the well-studied cases of point defect-related anelastic relaxation, e.g., hydrogen in metals^[18] or carbon in steel.^[19] In these materials, which display the Snoek effect, relaxation times fall within a range corresponding to a few Hz–kHz. Therefore, the method most commonly used to detect anelasticity in these materials is by measuring the imaginary component of the elastic modulus (i.e., internal friction) with a dynamic mechanical analyzer (DMA) (see for instance ref. [20]). However, anelastic relaxation times in the case of doped or reduced ceria can cover a usually broad range, from milliseconds to many weeks, thereby rendering DMA measurements unsuitable, even in view of the fact that the latest generation of DMA instruments can work at frequencies as low as 10 mHz. Nevertheless, in spite of these difficulties, there are data indicating that the relaxed elastic moduli of Gd-doped ceria are considerably smaller than the unrelaxed moduli.^[21–23]

2.2. Unrelaxed Elastic Moduli of Undoped and Gd-Doped Ceria

What may be termed the unrelaxed elastic (Young's) modulus corresponds to a time regime in which measurement of an anisotropic stress-imposed strain is made more rapidly than structural relaxation can occur.^[12] By contrast, the relaxed modulus can only be measured after sufficient time has passed that the point defect elastic dipoles are in equilibrium with mechanical and thermal constraints.^[12] However, doped ceria displays a wide range of relaxation times: milliseconds,^[24–26] seconds, or even months.^[10,11,21,27] To determine the unrelaxed modulus of Gd-doped ceria ceramics (reviewed in ref. [8]), a technique allowing rapid yet accurate measurement is required. Therefore, values of the Young's and shear moduli obtained with the impulse excitation technique or ultrasonic pulse-echo (USPE) measurement of sound velocity (SV) should approximate most closely the unrelaxed moduli. IET measures individual resonant frequencies of the ceramic, which depend on the

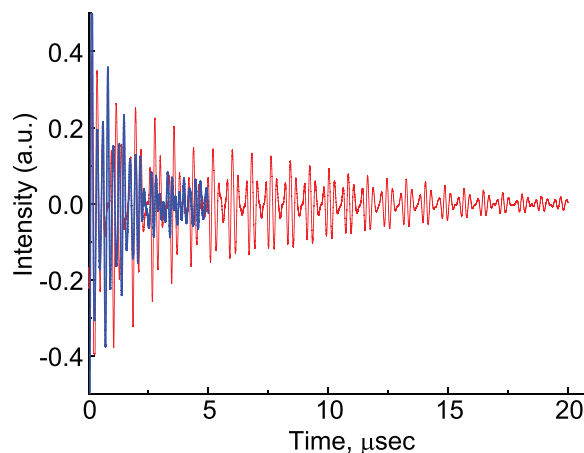


Figure 1. Time decay of an ultrasound pulse echo (shear wave) in two samples of 10 mol% Gd-doped ceria ceramics. Both samples are dense ($96.8 \pm 0.2\%$ theoretical) with an average grain size of $\approx 3 \mu\text{m}$. When samples contain a porosity of $\leq 6 \text{ vol}\%$, correction algorithms can be applied. However, the data quality is irreparably damaged by the presence of microcracks: the sample giving the blue trace is completely unsuitable for the measurement of elastic moduli. However, because of the visual nature of the data wave forms, those samples with microcracks can be identified and eliminated from analysis.

particular mode excited, sample density and dimensions: for a centimeter-sized sample both shear and flexure mode frequencies are typically a few hundred kHz. USPE uses shorter pulses and measures sound velocity via round trip travel time. The IET method has a significant advantage in that it can be implemented at temperatures above ambient. However, both IET^[28] and USPE^[9] must be corrected for porosity, and measurements are not reliable if ceramic porosity exceeds 6 vol%. Porosity of 21 vol% reduces the elastic modulus by a factor of 2.^[29] In addition, neither technique can compensate for the presence of microcracks (viz. **Figure 1**). Unfortunately, there have been a few measurements of elastic moduli of Gd-doped ceria using IET or USPE. In 2000, Atkinson and Selcuk^[28] reported Young's moduli and Poisson ratios for 10GDC: 200 GPa and $\nu_{10\text{GDC}} = 0.328$, and for 20GDC: 187 GPa and $\nu_{20\text{GDC}} = 0.334$. The values of the elastic moduli are significantly lower than those reported recently by Yavo et al.^[9] for 10GDC: $215 \pm 1 \text{ GPa}$ and $\nu_{10\text{GDC}} = 0.314 \pm 0.003$, and for 20GDC: $206 \pm 1 \text{ GPa}$ and $\nu_{20\text{GDC}} = 0.313 \pm 0.002$, respectively. The origin of this discrepancy is not known; however, a possible cause is the presence of microcracks. Microcracks can be present even in a very dense ceramic. While their influence can be signaled by the early decay of the ultrasound pulse (Figure 1), and thereby result in the removal of a particular sample from consideration; numerical correction for their influence is not currently available for either IET- or SV-based techniques. However, because of the visual nature of the USPE data wave forms (Figure 1), those samples with microcracks can be identified and eliminated from analysis.

The unrelaxed Young's and shear moduli of dense ceria ceramics decrease linearly within the range of stability of the fluorite phase $\text{Ce}_{1-x}\text{Gd}_x\text{O}_{2-x/2}$ ($x \leq 0.2$)^[9] with $4.8 \pm 0.3\%$ reduction in the normalized values for each additional 10 mol% Gd. The values for Young's and shear moduli for $x = 0.29$ (the double fluorite phase) are larger than expected from the linear

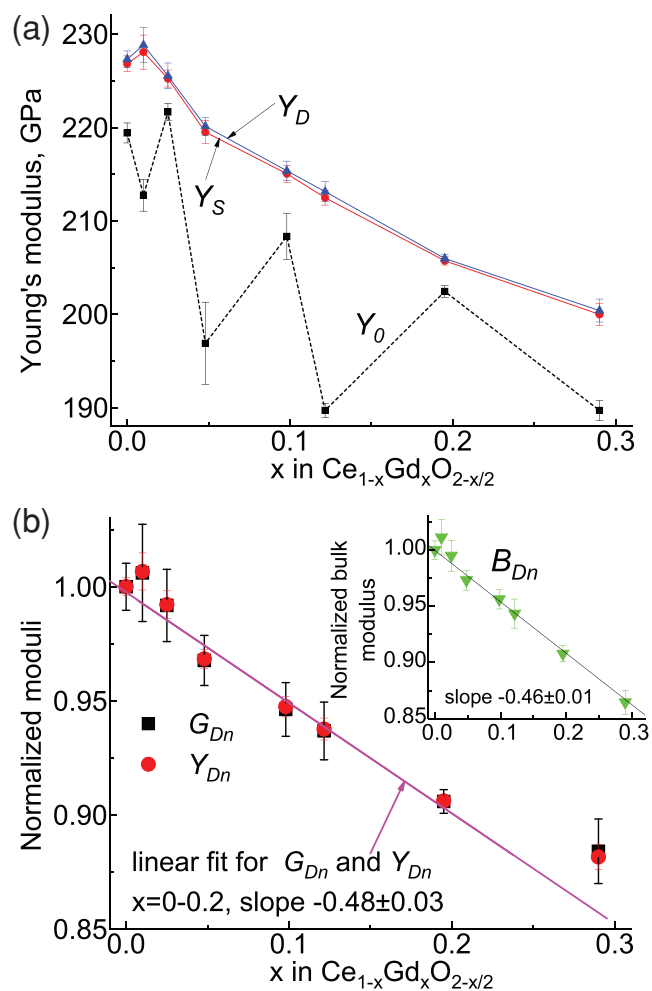


Figure 2. a) Young's modulus of ceria ceramics under ambient conditions as a function of Gd doping. Moduli were calculated from ultrasound pulse-echo velocity measurements: without correction for porosity, Y_0 , and including correction for porosity according to static, Y_S , and dynamic models, Y_D . b) Young's (Y_{Dn}), shear (G_{Dn}), and bulk moduli (B_{Dn}) corrected for porosity according to the dynamic model and normalized to the undoped values, as a function of Gd content. Linear regression gives the same slope for Young's and shear moduli within the fluorite phase ($x \leq 2$). However, the values for $x = 0.29$ (double fluorite phase) clearly cannot be included. On the other hand, for the normalized bulk modulus (inset) there is no such deviation. Adapted with permission.^[9] Copyright 2016, Elsevier.

decay. The bulk modulus also decays linearly with a similar slope of 4.6% per 10 mol% Gd but also including the composition $x = 0.29$ (Figure 2). We conclude from the USPE observations^[9] that the onset of ordering of oxygen vacancies during the transition from the fluorite to the double fluorite phase does not affect the response of the lattice to isostatic deformation, i.e., the bulk modulus. Suggested structural origins for the decrease of the unrelaxed elastic moduli with dopant concentration include increase in the volume of the unit cell as well as the reduction in the number of cation–anion bonds.^[30–32] We also note that while it is possible to measure the unrelaxed modulus with nanoindentation,^[10,11] the accuracy of this method (typically $\pm 5\%$) is considerably lower than IET or SV. Therefore, it does not detect

the dependence of the elastic moduli on Gd content.^[10] Moreover, specifically for doped ceria, nanoindentation measurements are complicated by anelastic effects, as discussed below.

2.3. Anelastic Effects in Gd-Doped Ceria

2.3.1. Relaxed Biaxial Elastic Modulus of Gd-Doped Ceria Thin Films

Evidence that the relaxed biaxial elastic modulus of Gd-doped or reduced ceria thin films is considerably lower than the unrelaxed one dates to 2010.^[23,33] These reports showed that substrate-supported thin films of $\text{Ce}_{0.8}\text{Gd}_{0.2}\text{O}_{1.9}$ or oxygen-deficient, undoped ceria can sustain in-plane strain of 0.2–0.3%, as measured by XRD, while the stress determined from measuring the curvature of the substrate does not exceed 30 MPa (the detection limit for 250 μm thick Si substrates). The films are polycrystalline and more than 400 nm thick, which indicates that epitaxy is not responsible for such behavior. The biaxial elastic modulus Y_b estimated from these data is < 17 GPa, which is more than 10 times lower than the calculated biaxial elastic modulus for bulk 20GDC: 300 GPa.^[9] Thin substrate-supported films of Gd-doped ceria retain large in-plane strain even after prolonged annealing at elevated temperatures.^[7,34] This strain is not plastic: partial substrate removal produces a self-supported film (membrane), which is strongly buckled. For instance, in Shi et al.,^[34] the reported strain is 0.45%, and in Kossoy et al.,^[33] it is 0.3%. The formation of buckled membranes provides evidence that the large strain in substrate-supported films is recoverable. We note that elastic strain of this magnitude for 20GDC would produce in-plane stress $\sigma = Y_{b20\text{GDC}} \cdot 0.45\% = 1.35$ GPa. To maintain such stress in a 1 μm thick film, the adhesion energy would have to exceed 1 J m^{-2} ,^[35] which is unlikely for a polycrystalline, nonepitaxial film: rather, delamination (blistering) would result. However, in practice, that is not observed for thin films of 20GDC.

There are serious practical consequences of these observations. The driving force for strain relaxation is the amount of elastic energy stored, i.e., stress. Since, as we have described above, the “relaxed” biaxial modulus of Gd-doped ceria films is a small fraction of the unrelaxed modulus, stress in the films is low, resulting in insufficient driving force for strain relaxation. Heating for longer than 10 h above 500 $^\circ\text{C}$ would provide partial strain relief; however, as noted in the introduction section for Si substrate-supported films, the difference between the thermal expansion of Gd-doped ceria and Si over this temperature range is $\approx 0.38\%$. Therefore, the structural integrity of the films will be compromised after thermal cycling to room temperature due to the resulting tensile strain. Obviously, the thermal treatment necessary for complete strain relaxation in ceria thin films must be tailored for each case on an empirical basis, e.g., as described in Kossoy et al.^[21]

2.3.2. Hysteresis of the Lattice Parameter of Thermally Cycled Gd-Doped Ceria Thin Films

A broad range of values have been reported in the literature for the unit cell dimension (a) of Gd-doped ceria for $x \leq 0.2$ ^[36–40] (Figure 3). In the case of substrate-supported thin films, such

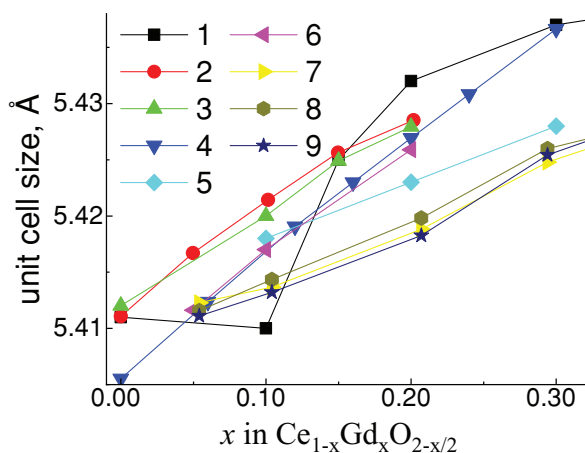


Figure 3. Cubic unit cell (*Fm-3m*) lattice parameters reported in the literature for different doping levels $\text{Ce}_{1-x}\text{Gd}_x\text{O}_{2-x/2}$: 1, ref. [36]; 2, ref. [37]; 3, ref. [38]; 4, ref. [39]; 5, ref. [40]; 6, ref. [21]; 7–9, ref. [88] at 550, 750, and 1100 °C, respectively. Adapted with permission.^[21] Copyright 2009, Wiley-VCH.

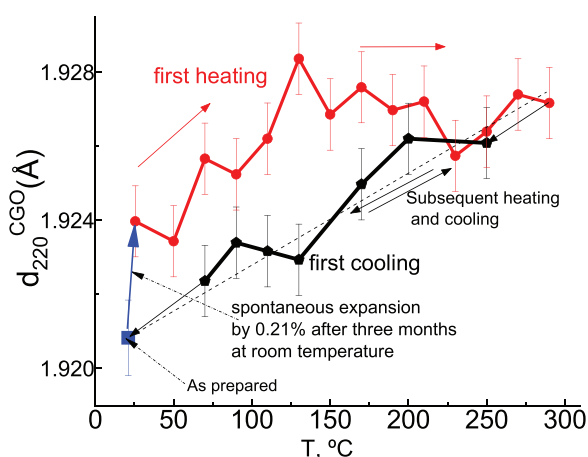


Figure 4. d -Spacing of the 220 X-ray diffraction peak of a 330 nm thick film of $\text{Ce}_{0.8}\text{Gd}_{0.2}\text{O}_{1.9}$ deposited by sputtering on a Si substrate and measured as a function of temperature between 25 and 300 °C. Following annealing at 530 °C and subsequent thermal cycling, the XRD measurements of the out-of-plane lattice parameter were made under ambient conditions prevailing in the X-ray laboratory. Adapted with permission.^[21] Copyright 2009, Wiley-VCH.

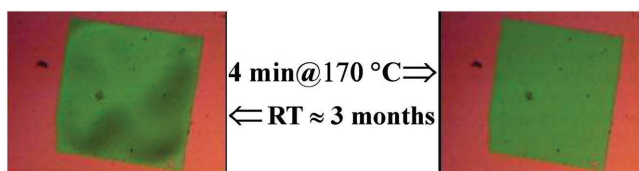


Figure 5. Light microscopy images of a self-supported film of $\text{Ce}_{0.8}\text{Gd}_{0.2}\text{O}_{1.9}$ (470 nm thick). Upon removal of the substrate, the film buckles. Upon heating the membrane to 170 °C for 4 min, the buckling is eliminated. After 3 months at room temperature, the membrane spontaneously rebuckles. The cycles of flattening/buckling can be repeated multiple times. Adapted with permission.^[21] Copyright 2009, Wiley-VCH.

differences might be explained by the presence of in-plane deposition strain. However, the data in Figure 3 refer to ceramics, which are presumably strain free: the spread in the fractional change in the lattice constant as a function of dopant concentration exceeds 0.25%. In powders and ceramics with micrometer-sized grains, extrinsic effects such as macroscopic strain, surface reduction, oxygen concentration gradient, and/or contribution of the grain boundaries are minimized. This suggests that, in addition to extrinsic effects, there is another factor affecting the lattice parameter of GDC. A possible source of this scatter was identified by showing that the lattice parameter of Gd-doped ceria thin films—both substrate-supported and self-supported—increases spontaneously over the course of a few months. The out-of-plane d -spacings of the 220 diffraction peak (Figure 4) were measured at room temperature (23 ± 2 °C) on a 330 nm thick 20GDC film that had been deposited by RF magnetron sputtering directly on Si and annealed in air for 12 h at 530 °C.^[21] This annealing protocol had previously been found to minimize sample strain for films deposited on Si. Nevertheless, the films retained compressive strain of 0.19–0.37%. After annealing and over the course of three months at room temperature, the out-of-plane lattice parameter increased spontaneously by 0.21%. Interestingly, the first heating following this prolonged dwell at room temperature did not produce the expected lattice expansion between 150 and 300 °C. However, cooling did return the lattice constant to approximately the same value that was observed prior to the spontaneous expansion. Subsequent cooling and heating cycles produce thermal expansion corresponding to $\pm 11 \times 10^{-6} \text{ K}^{-1}$, which is the value commonly observed for bulk $\text{Ce}_{0.8}\text{Gd}_{0.2}\text{O}_{1.9}$.^[3,22] Three-month dwell under ambient conditions causes the lattice to expand once more by $\approx 0.2\%$. Even more striking is the behavior of a self-supported 20GDC film, as described in Kossoy et al.^[21] (Figure 5). The initially flat, supported film acquires a buckled shape upon substrate removal. Heating for 4 min at 170 °C flattens the film. During three months under ambient conditions, the film rebuckles. This flattening/buckling cycle can be repeated multiple times. Gd-doped ceria films have been shown to be resistant to possible structural influences of water and CO_2 ;^[41] therefore, the hysteresis of the lattice parameter cannot be attributed to simple physical or chemical degradation.

Clearly, the lattice parameter of Gd-doped ceria thin films is a function of sample history, including time, applied stress, and temperature. Therefore, the unit cell dimensions of two samples prepared at different times or kept under different conditions are not comparable. As a result, a well-defined value of the unstrained lattice parameter a_0 is not available. This creates difficulties in evaluating the in-plane and out-of-plane strains, u_{xx} and u_{zz} , respectively, of such thin films; XRD measurements of the in-plane, a_x , and out-of-plane, a_z , lattice parameters are insufficient; rather a well-defined value of either the unstrained lattice parameter, a_0 , or the Poisson's ratio, ν , must be provided

$$u_{xx} = \frac{a_x - a_z}{a_z + 2 \cdot a_x \cdot \nu} \quad (\text{if } \nu \text{ is known}) \quad \text{or} \quad u_{xx} = \frac{a_x}{a_0} - 1 \quad (\text{if } a_0 \text{ is known}) \quad (1)$$

For linear, elastic materials, a_0 and ν do not change with time or strain. However, for anelastic materials, such as 20GDC films, it is apparently not so. This is also apparent in

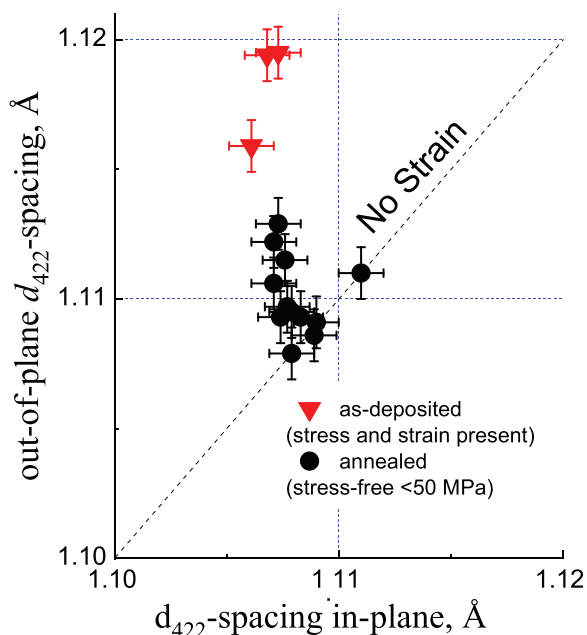


Figure 6. Values for the in-plane and out-of-plane d_{422} -spacing for thin films of $\text{Ce}_{0.8}\text{Gd}_{0.2}\text{O}_{1.9}$. Adapted with permission.^[42] Copyright 2014, Springer.

Figure 6, which is adapted from Kossoy et al.,^[42] in which the out-of-plane d_{422} -spacing and in-plane d_{422} -spacing for 13 as-sputtered and annealed films are compared. The differences in the a_z/a_x ratio are well outside the range of uncertainty of the XRD measurement.

2.3.3. The Poisson's Ratio of Gd-Doped Ceria Thin Films

Measuring the Poisson's ratio of materials that may have a relaxation time as long as a few weeks following the development of strain is very challenging. Since the Poisson's ratio is defined as the ratio between two small quantities, $-u_{xx}/u_{zz}$, achieving acceptable accuracy requires imposing large strain (at least one-tenth of a percent) and maintaining this strain for a period of time sufficient for the defect equilibrium to reestablish. Ceramics are rarely capable of withstanding large deformation without cracking. A partial solution for this problem using X-ray diffraction measurements was provided in Goykhman et al.^[43] A film is deposited on a flexible substrate, and the in-plane and out-of-plane d -spacings of a given set of lattice planes are measured in the initially "flat" state, d_x^f and d_z^f , respectively. The difference in these values is the characteristic of the deposition strain. Then, the substrate is bent with a predetermined radius, R , and the d -spacings are measured in this "bent" state d_x^b and d_z^b (**Figure 7a**). Bending introduces additional strain in the film which can be calculated as $u_{xx}^R = t_s/(2R)$, where t_s is the thickness of the substrate. For a 100 μm thick substrate bent with a radius of 50 mm, the additional film in-plane strain is 0.1%, assuming perfect adhesion, which is sufficient to detect the difference in lattice spacings between the "flat" and the "bent" state. In practice, some relaxation will take place; therefore, u_{xx}^R is more accurately $(d_x^b - d_x^f)/d_x^f$. The total in-plane

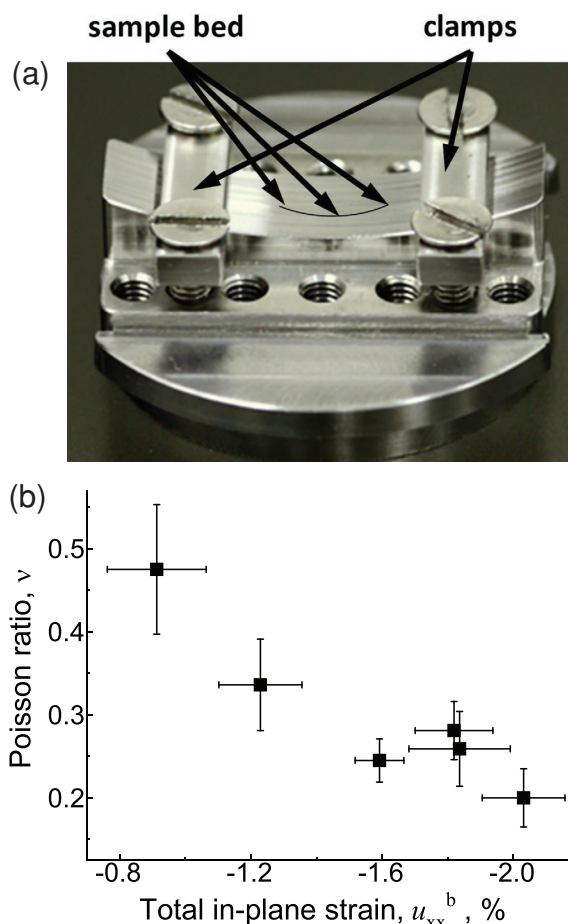


Figure 7. a) Device for bending thin film samples deposited on flexible phosphor bronze substrates to a predetermined radius of 50 mm and which could be mounted in the Rigaku TTRAXIII diffractometer. The sample is clamped to the convex bed as shown. b) Poisson ratio, ν , of $\text{Ce}_{0.8}\text{Gd}_{0.2}\text{O}_{1.9}$ thin films as a function of the total in-plane strain (u_{xx}^b), where $u_{xx}^b = u_{xx}^f + u_{xx}^R$, b indicates bent, f indicates flat, and u_{xx}^R is the strain imposed by bending the substrate. Adapted with permission.^[43] Copyright 2014, Springer.

strain in the bent state u_{xx}^b is taken to be the sum of u_{xx}^f and u_{xx}^R . When the bending radius, R , is much larger than the substrate thickness (as in this case), no strain will be introduced in the direction of the bending axis. Knowledge of the exact value of the bending strain is not crucial; however, larger u_{xx}^R will increase measurement accuracy. The Poisson's ratio can be approximated from the lattice interplane spacings as^[43]

$$\nu = \frac{d_z^b - d_z^f}{d_z^b - d_x^b + d_x^f - d_z^f} \quad (2)$$

Since the bending strain is generally significantly smaller than the deposition strain present in the flat film, Equation (2) is derived by removing terms quadratic in the strain.^[43] For this experimental arrangement, the error introduced by this approximation is $\approx 2\text{--}3\%$ both for the Poisson's ratio and for the in-plane strain in the flat state. Even given the rather large uncertainty in the data from six 20GDC films (**Figure 7b**), which propagates from the uncertainty in the profile fitting of

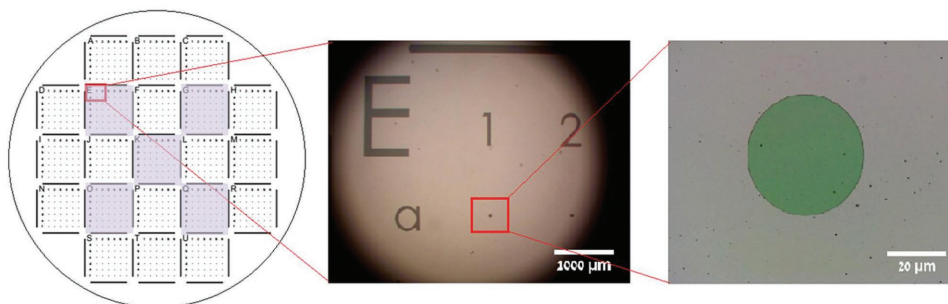


Figure 8. A Cr mask deposited on the GDC film enabled reproducible monitoring of the Raman scattering measurements from well-defined positions. a) The mask fabricated on a 2 in silicon wafer. The highlighted areas in Figure 9 are referred to as E, G, K, O, and Q. b) Optical microscopy image showing indexing of individual locations in area E (a–g; 1–7). c) Optical microscopy image shows a 40 μm diameter circle of exposed GDC surrounded by the Cr mask. Adapted with permission.^[27] Copyright 2017, Elsevier.

the XRD peak positions, Poisson's ratio clearly decreases with increase in total in-plane strain (Figure 7). When $u_{xx}^b < 1\%$, the film appears to approximately preserve volume under strain, i.e., $\nu = 0.47 \pm 0.08$. Upon increase of the in-plane strain, ν decreases to $\approx 0.2 \pm 0.035$ ^[43] indicating that communication between deformation in different directions in the crystal lattice is weak. Although strain-sensitive Poisson ratios are not common, this behavior has in fact been observed in various biological materials and synthetic polymers.^[44] We also note that the fact that elastic anisotropy, possibly deriving from preferential (111) orientation of the fluorite lattice in the deposited film crystallites, may be influencing these results.

2.3.4. Influence of Mechanical Relaxation on Raman Spectra

Raman spectroscopy has been used to detect the presence of strain and point defects in ceria via the position, line width and asymmetry of the F_{2g} vibrational mode (symmetric breathing mode of the eight anions near neighbor to the cation), as well as the appearance of other cubic symmetry forbidden vibrational modes. In Shi et al.,^[34] Raman spectra were monitored to determine local strain in membranes of $Ce_{0.8}Gd_{0.2}O_{1.9}$. The in-plane strain in these membranes was deduced from the curvature of the films obtained by surface profile measurements. In view of the foregoing discussion of the anelastic properties of Gd-doped ceria, it is not obvious that the Raman F_{2g} peak position is in fact a reliable measure of strain in GDC thin films or membranes. Moreover, analysis of Raman spectra involves separating the effect of lattice expansion due to dopant incorporation from changes in chemical bonds. This approach dates to 1994^[45] and since then it has been used frequently (for example, refs. [46,47]). The implicit assumption is that the fractional increase in the unit cell volume, $\Delta V/V$, can be related to the relative shift in the position of a Raman peak, $\Delta\omega/\omega$, as

$$\frac{\Delta\omega}{\omega} = \gamma \cdot \frac{\Delta V}{V} \quad (3)$$

where γ is the Grüneisen parameter for the corresponding Raman vibrational mode. The value of γ obtained for the case of isostatic compression in ceramic samples is approximately constant. Although there is some spread in the literature data,

for bulk samples, γ is usually reported to be 1.17–1.41 for 10GDC and 1.24^[46,47] or 1.5 for undoped ceria with reference to the study of high-pressure isostatic compression.^[48] This implies that, for instance, the most intense Raman peak of ceria, F_{2g} at 465 cm^{-1} , will shift by 1 cm^{-1} if the volume change reaches 0.2%. For a material with bulk modulus of $\approx 200 \text{ GPa}$,^[9] this requires 0.4 GPa pressure. In Kraynis et al.,^[27] it was shown that in Raman spectra of thin films of 5 and 10 mol% Gd-doped ceria substrate-supported films, the position of the F_{2g} peak is not constant with time. 400 nm thick films were deposited by RF magnetron sputtering in a mixed oxygen/Ar atmosphere in order to prevent oxygen loss. The Si substrate was covered with a 500 nm thick Ti layer to promote adhesion, facilitate strain relief, and avoid interference by the strong Raman peaks of Si. The films were annealed for 4 h at 400 °C to relieve deposition stress. Despite the presence of the Ti layer, annealing does not completely relieve strain; the out-of-plane/in-plane anisotropy $((a_z/a_x) - 1)$, where a_z is the out-of-plane lattice constant and a_x is the in-plane lattice constant as measured by XRD at the film center (K point), is reduced from 0.48% and 1.0% to 0.13% and 0.3% for 5GDC and 10GDC, respectively. However, because metallic Ti undergoes plastic relaxation at 400 °C, the residual strain is much lower than for the films deposited directly on Si (see Section 2.3.2 and Kossoy et al.^[21]). To monitor the F_{2g} peak over time at precisely the same locations, a patterned and labeled grid of 40 μm holes was created in a Cr layer that had been deposited on the GDC films (Figure 8). It was found that even though the XRD lattice parameters measured at the film center (K) and therefore the volume of the unit cell did not change during the weeks following annealing, the positions of the F_{2g} Raman peaks (Figure 9) continued shifting for almost two weeks for 5GDC and six weeks for 10GDC. We note that for 5GDC, the Raman F_{2g} peaks shift toward higher energies by more than 0.5 cm^{-1} . According to Equation (3), the volume of the unit cell should decrease by at least $0.5/458/1.5 \approx 0.07\%$. Taking into account that the films are clamped to the substrate, this decrease should come at the expense of out-of-plane unit cell dimensions. Such a large change should be detectable. However, in the absence of any change in the 5GDC lattice parameters at the film center (position K) during 2 weeks, the shift in the Raman F_{2g} peak position has been attributed to the reorganization/redistribution of local strain fields of elastic dipoles, when the residual strain/stress is anisotropic, as it is

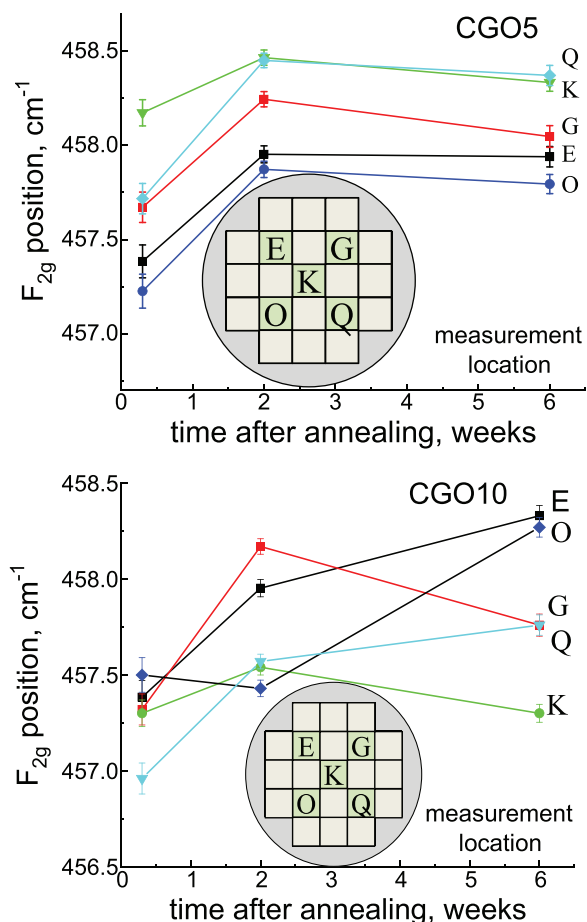


Figure 9. Shift of the position of the Raman F_{2g} peak position, shortly following, two weeks, and six weeks after, and annealing of 5% and 10% Gd-doped ceria thin films deposited on Si. No change in the average out-of-plane lattice parameter at location K was recorded by X-ray diffraction for either sample. Adapted with permission.^[27] Copyright 2017, Elsevier.

here. According to classical understanding of anelasticity,^[12] this is the origin of a time-dependent relaxation process. These data^[27] restrict use of the concept of a Grüneisen parameter for determining anisotropic strain in ceria thin films because, as a result of cation doping and/or oxygen vacancy creation, the unit cell volume and the stiffness of the bonds are not directly linked. Since, as described above, the biaxial elastic moduli of ceria membranes and ceramics are very different, therefore different values of the Grüneisen parameter should be used for strain analysis of thin films^[34,49] or bulk ceramics.^[49] However only for the latter literature values are available.^[48,50] A new approach for using micro-Raman spectroscopy to monitor strain in thin films of ceria would therefore be most welcome.

2.4. Room-Temperature Creep in Ceria Ceramics

Creep, or the time-dependent yielding of a solid under constant load, constitutes a difficult problem in material characterization and application. Creep strain reaches a plateau for an anelastic solid while it continues to increase for a viscoelastic solid. In the particular case of linear anelastic materials, complete

recovery is eventually achieved upon removal of external stress. Although creep is generally observed in ceramics only when the temperature is raised toward the material melting point, room-temperature creep has in fact been detected in ceria ceramics using the nanoindentation (ND) technique.^[10,11]

Nanoindentation is a popular technique for measuring microhardness and Young's elastic modulus (E) of ceria ceramics^[10,11,51,52] and less commonly, supported thin films.^[53,54] Room-temperature ND measurement (loading/unloading rate 0.1–0.5 mN s⁻¹; max. load 1–5 mN) of the Young's modulus of CeO_{2-δ} and Pr_{0.2}Ce_{0.8}O_{2-δ} thin films, deposited by PLD on single crystal YSZ substrates, gave 264.6 and 276.5 ± 7.7 GPa, respectively. These magnitudes agree well with reported values of E measured by nanoindentation under similar conditions for bulk samples of Pr_{0.2}Ce_{0.8}O_{2-δ} (274 ± 25 GPa) and undoped ceria ceramics (264.1 ± 2.2 GPa)^[51] (loading/unloading rate 1 mN s⁻¹; max. load 5 mN).

Ceramics used for nanoindentation measurements must satisfy a number of requirements. 1) In order that the properties of the surface layers probed by the indenter be representative of the bulk material, final polishing must be performed with a very fine powder (e.g., 20 nm particle size) for a period of time sufficient to remove surface layers damaged by coarse powders. 2) The ceramic grain size should be sufficiently large that indentation may be confined to one grain and therefore material elastic modulus and microhardness will not be influenced by ceramic porosity. We note that Morales et al.^[52] also included up to 2 wt% cobalt acetate to facilitate sintering the Ce_{1-x}Gd_xO_{2-x/2} pellets. In Korobko et al.,^[10,11] Gd-, Lu-, Pr(III)-, and Pr(IV)-doped ceria ceramics with grain size >1.5 μm were subjected to indentation with Berkovich (three-sided pyramidal diamond) indenter under constant loading rates of 15 or 0.15 mN s⁻¹ (Figure 10a). The standard ND procedure is as follows: loading at a constant rate, hold at constant load, and followed by constant rate unloading, with E determined by linear fit to the initial slope of the unloading curve on the load/displacement graph, after correcting for the properties of the indenter and assuming a value for the Poisson's ratio of the sample. However, the results obtained with the ×10² slower loading rate presented very large margins of error. Following rapid loading, displacement continually increased during load hold at 150 mN (a factor of 30 higher load than reported in Wang et al.^[51]), i.e., the ceramics exhibited room-temperature creep. The displacement, u , during creep was fitted to $u = u_0 + A(t - t_0)^{1/3}$, where A is the creep magnitude parameter, and $(t - t_0)$ is elapsed time from beginning of load hold. The (primary) creep parameters provide informative constraints on the origin of the room-temperature creep. During load hold, the applied stress reached 10 GPa (i.e., 150 mN on a 3 μm diameter grain), which is ≈10% of the shear modulus and less than 5% of the elastic Young's modulus) and the maximum indentation depth is less than half the average grain size. Under such conditions, material transfer by diffusion at grain boundaries cannot produce the ≈10 nm displacement observed within a few seconds: cation diffusion in ceria is only significant above 1000 °C.^[55] Moreover, dislocation movement, if it occurs, should be obstructed by the dislocation pinning of the dopants: the larger the difference between the crystal radii of the dopant and that of the host, the lower the creep. However, for 3 mol% of the larger dopants, Gd³⁺

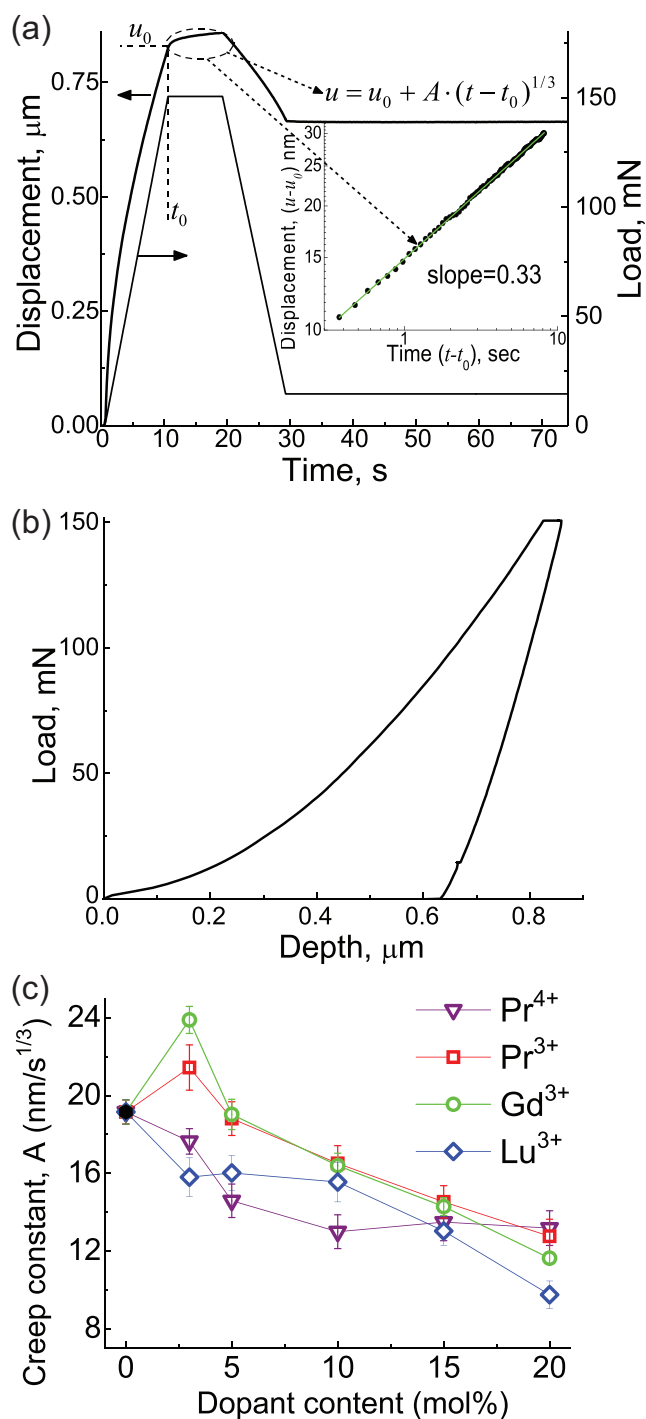


Figure 10. a) Displacement–time and load–time dependence for “fast” nanoindentation loading (15 mN s^{-1}) of a ceria pellet with 10 mol% Gd. Inset: The log–log plot of displacement versus time during the hold phase, indicating that the displacement is proportional to $t^{1/3}$. b) Typical displacement (depth)–load curve. c) Creep rate constant for Gd^{3+} , Pr^{4+} , Pr^{3+} , and Lu^{3+} -doped ceria from refs. [10]. Adapted with permission.^[10] Copyright 2013, Wiley-VCH.

and Pr^{3+} produce an increase in the creep rate while the same doping level with Lu^{3+} and Pr^{4+} suppresses creep (Figure 10c). Therefore, room-temperature creep in ceria ceramics has been

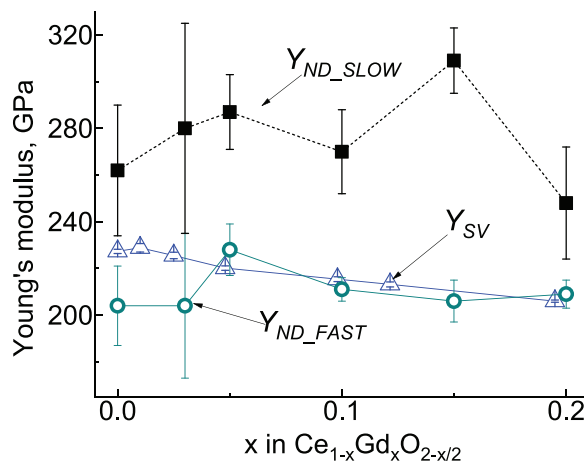


Figure 11. Comparison of the values of the Young's modulus obtained by nanoindentation^[11] and ultrasonic pulse-echo sound velocity (USPE SV) measurements as a function of Gd doping in dense ceria ceramics.^[9] The SV measurements have been corrected for porosity. Figure 11 is plotted from data in ref. [9] and ref. [11]

attributed to the rearrangement of elastic dipolar strain fields associated with lattice point defects in response to anisotropic stress. Creep suppression sets in at dopant concentrations above 3 mol%, likely due to interaction of point defect strain fields. We note that for the case of the two smaller dopants, Lu^{3+} and Pr^{4+} , the creep rate constant is lower than that of undoped ceria and for Pr^{4+} only weakly dependent on dopant concentration (Figure 10c). The origin of creep in undoped ceria is attributed to the reduction of Ce from +4 to +3 accompanied by the creation of charge compensating oxygen vacancies.

Room-temperature creep affects the values of the Young's elastic modulus calculated from the initial slope of the load release curve and the indenter contact area. As noted above, for all dopants only the results obtained with the fast loading were considered to be reliable. However, even those data have significantly larger error margins than the elastic moduli determined from the USPE SV data^[9] described above. If we compare the values of the Young's modulus for Gd-doped ceria, $x = 0.05\text{--}0.2$ (Figure 11), obtained by ND and SV measurements, we see that indeed the mean values of the Young's modulus extracted from the fast loading ND measurements are quite close to those obtained by the SV method after correction of the latter for ceramic porosity.

There are a number of interdependent, structural parameters that influence the magnitude of the Young's elastic modulus determined by ND under rapid loading as a function of dopant concentration 0–20 mol% in Gd^{3+} , Pr^{3+} , Lu^{3+} , or Pr^{4+} -doped ceria ceramics (Figure 12). These include the increase or decrease in the fluorite lattice constant of the solid solution with increasing dopant concentration (Vegard's law), the crystal (ionic) radii of the dopant and host cations with coordination numbers 6 or 8, the redox status of the host cation and perhaps in the case of Pr^{4+} (accomplished by annealing the Pr^{3+} ceramics in oxygen for 12 h at 380°C), also of the dopant; and the appearance of charge compensating oxygen vacancies of (currently) unknown size. In this context, we note that the preparation of completely oxidized, undoped ceria ceramics is very challenging. Since for undoped ceria, the oxygen self-diffusion coefficient does not exceed $10^{-14} \text{ cm}^2 \text{ s}^{-1}$ at

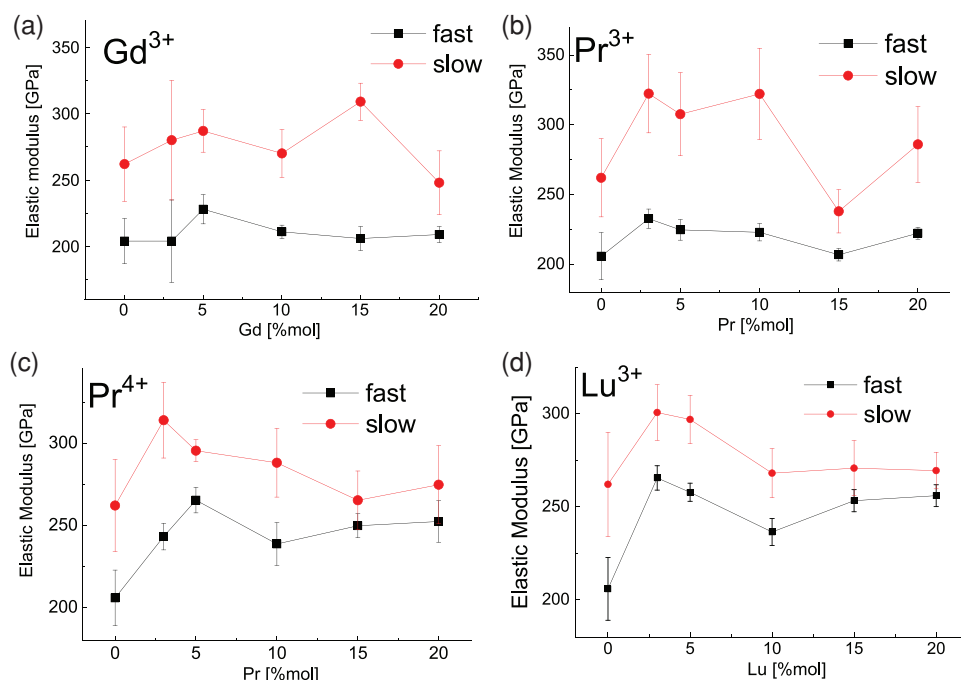


Figure 12. Nanoindentation measurement of the elastic (Young's) modulus of ceria ceramics as a function of doping derived from rapid loading/unloading to 150 mN (15 mN s⁻¹, 8 s hold) and slow loading/unloading (0.15 mN s⁻¹, 30 s hold). The data for Pr⁴⁺, Pr³⁺, and Lu³⁺-doped ceria (b–d) are from ref. [10]. The data for Gd³⁺-doped ceria (a) are from ref. [11]. Adapted with permission.^[10] Copyright 2013, Wiley-VCH.

575 °C,^[56] even if the ceramic is annealed for 1 week in oxygen at 575 °C, the diffusion depth will not be greater than ≈1 μm. The lattice constants of the ND sample ceramics, as measured by X-ray diffraction under ambient conditions, increased in the concentration range 0–20 mol% for Gd³⁺ and Pr³⁺ while a decrease was observed for Lu³⁺ and Pr⁴⁺ doping.^[10] Numerous X-ray absorption measurements provide evidence that, even in this limited doping range, fluorite symmetry is only maintained on the basis of temporal and spatial averaging.^[16,23,33,46,57] The crystal radii of the host and dopant cations decrease/increase by ≈10 pm when the coordination numbers change from 8 ↔ 6. The decrease in the coordination number in these ceramics can be ascribed to the appearance of oxygen vacancies. A 10 pm decrease takes place for cations undergoing oxidation when the valence changes from +3 to +4. Ionic radii display the same variability as crystal radii although the absolute sizes are smaller.^[58] Since the elastic Young's constants of the doped ceria grains, as well as the primary creep constants, display complex behavior as a function of doping, while the determining structural parameters also do not remain unchanged, a definitive explanation of the ND results is not yet in hand.

3. Electromechanical Activity of Ceria Films and Ceramics

3.1. Classical versus Nonclassical Electrostriction

Piezoelectricity, i.e., the linear electromechanical response, is restricted to noncentrosymmetric materials. However, materials with nonlinear electromechanical response have drawn increased attention during the last two decades.^[59,60]

Electrostriction, the simplest nonlinear response, is second order (quadratic) with respect to the electric field and it is displayed by all types of dielectric materials irrespective of crystal symmetry or structure.^[59] In a general form, it is described by a fourth-rank tensor, M_{ijmn} , relating the strain components, u_{ij} , to the component of the electric field, E_n, E_m

$$u_{ij} = \sum_{n,m} M_{ijmn} E_n E_m \quad (4)$$

The values of the electrostriction strain coefficients, M_{ijmn} , vary from 10⁻²¹ to 10⁻¹⁶ m² V⁻² and can be both positive and negative, depending upon whether the material expands or contracts in the electric field.^[59,61–63] To rationalize these very different numbers, Newnham et al.^[59] introduced the polarization electrostriction coefficient, Q_{ijmn} , relating the field-induced strain to the dielectric polarization, P_k , or dielectric susceptibility, χ_{km} , rather than to the applied electric field $P_k = \sum_l \chi_{kl} E_l$

$$u_{ij} = \sum_{n,m} Q_{ijmn} P_n P_m \quad (5)$$

The polarization electrostriction coefficients are related to electrostriction strain coefficients as

$$M_{ijmn} = Q_{ijmn} \cdot \epsilon_0 \epsilon_{im} \cdot \epsilon_{jn} \quad (6)$$

which for the case of a material with cubic symmetry (ϵ_{im} , the dielectric constant tensor, is isotropic) becomes

$$M_{ijmn} = Q_{ijmn} \cdot [\epsilon_0 \cdot (\epsilon - 1)]^2 \quad (7)$$

where ϵ_0 is the permittivity of free space. Since materials have very different symmetries, Newnham et al.^[59] considered the

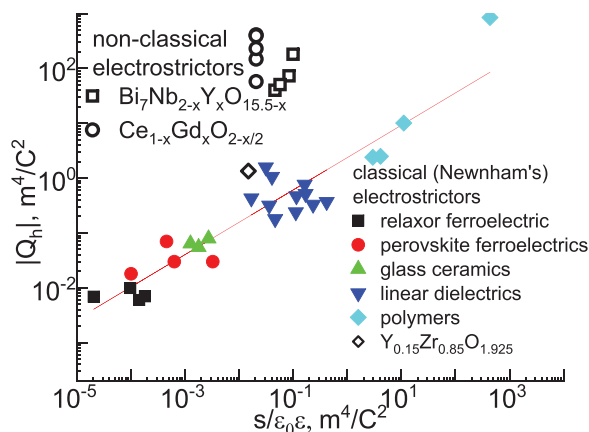


Figure 13. Hydrostatic polarization electrostriction coefficient, $|Q_h|$, as a function of the ratio of the elastic compliance, S , to the material dielectric constant, $\epsilon \cdot \epsilon_0$. The full symbols mark data from ref. [59]. The data for Gd-doped ceria thin films are from ref. [57]. The data for $\text{Bi}_7\text{Nb}_{2-x}\text{Y}_x\text{O}_{15.5-x}$, $x = 0.4, 0.8, 1.2, 1.6$, ceramics and the data for a single crystal of (100cut) $\text{Y}_{0.08}\text{Zr}_{0.92}\text{O}_{1.96}$ are from ref. [82]. The red line represents the scaling law for classical electrostrictors, Equation (8), from ref. [59]. Adapted with permission.^[82] Copyright 2016, Wiley-VCH.

hydrostatic polarization electrostriction coefficient, Q_h , which characterizes the change in volume. For isotropic or cubic materials, Q_h takes the form $Q_h = Q_{xxxx} + 2Q_{xyxy}$, where Q_{xxxx} and Q_{xyxy} are the longitudinal and transverse polarization coefficients, respectively. Plotting $\log(|Q_h|)$ versus $\log(S/\epsilon\epsilon_0)$, where S is the inverse Young's modulus (elastic compliance), ϵ_0 is the permittivity of free space, and ϵ is the material dielectric constant, all examined dielectrics, from polymers^[64–66] to relaxor ferroelectrics,^[59,67–69] were found to follow the empirical relationship (Figure 13)^[59]

$$|Q_h| \approx 2.37 \cdot (S/\epsilon\epsilon_0)^{0.59} \quad (8)$$

which indicates a fundamental connection between these properties. This relationship was interpreted as evidence for significant anharmonicity in the lattice response to elastic and dielectric perturbation. A similar correlation between $|Q_h|$ and thermal expansion coefficients is also observed.^[70] Materials that obey the scaling law in Equation (8) have been termed “classical electrostrictors.”

According to Newnham's scaling law (Equation (8)), Gd-doped ceria would not be expected to exhibit particularly large electrostriction. The dielectric constant of $\text{Ce}_{1-x}\text{Gd}_x\text{O}_{2-x/2}$ at low temperatures is almost independent of frequency from a few Hz to 1 MHz, $\epsilon_\infty < 28$.^[71] At elevated temperatures, ionic conductivity and contact effects contribute to the measurable polarization; however, from the data in Yavo et al.^[72] it is possible to estimate that even if the polarization of the grain boundaries and contacts is included, then $\epsilon_{0.5 \text{ Hz}} < 100$. $\text{Ce}_{1-x}\text{Gd}_x\text{O}_{2-x/2}$

has a large Young's modulus (206–227 GPa; Figure 11^[10,11]) and therefore a correspondingly small elastic compliance. Measuring both M_{xxxx} and M_{xyxy} with the same setup is usually quite challenging; however, for cubic symmetry, one can approximate $M_{xyxy} \approx -\nu M_{xxxx}$ and $Q_h = Q_{xxxx}(1 - 2\nu)$.^[73] Therefore, values of $|Q_h|$ estimated by Equation (8) are $|Q_h| \approx 0.01\text{--}0.03$ and the electrostriction strain coefficient estimated from Equation (7) would have order of magnitude $M \approx 10^{-20} \text{ m}^2 \text{ V}^{-2}$. The fact that the measured values of the electrostriction strain coefficient exceed this estimate by more than two orders of magnitude has given rise to the term “nonclassical” electrostriction, as described below.

3.2. Room-Temperature Electrostriction in Supported Thin Films of Gd-Doped Ceria

Measuring a strain electrostriction coefficient for substrate-supported films is difficult due to the fact that the films are clamped. However, one can readily determine the stress that develops in the film if the substrate is sufficiently thin^[74] (Figure 14a): stress developing in the film causes the cantilever to bend, thereby shifting the position of the reflected laser beam on the detector. Since stress rather than strain is measured, the method allows the determination of the electrostriction stress coefficient γ_{xyxy} , which is related to the strain coefficient via the corresponding elastic modulus. For the transverse coefficients $\gamma_{xyxy} = M_{xyxy} \cdot Y_b$, where $Y_b = Y/(1 - \nu)$ is the biaxial modulus. This technique has a number of advantages:

1. Using a CCD camera and mathematical processing, one can measure the movement, ΔX , of the reflected beam with an accuracy of at least 0.05 pixel of the CCD camera ($< 1 \mu\text{m}$), which is orders of magnitude smaller than the beam diameter (1 mm). The change in curvature of the cantilever can be found as given in Equation (9)^[74]

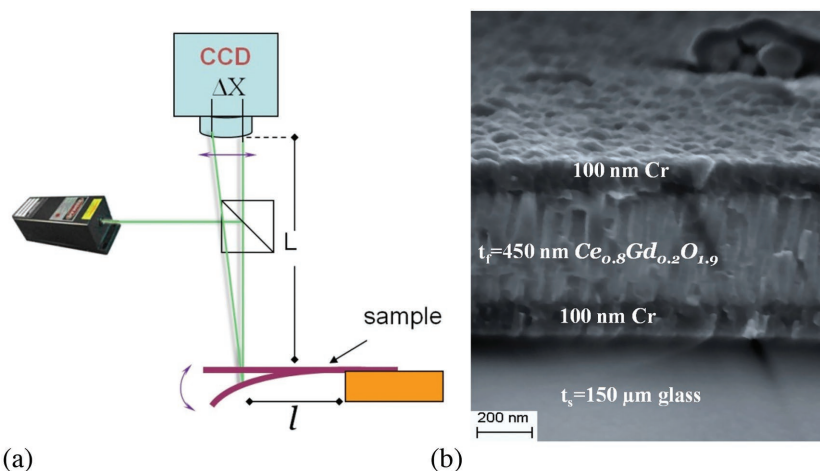


Figure 14. a) Electrostrictive response of a 20 mol% Gd-doped ceria (20GDC) thin film induces cantilever curvature. A change in curvature shifts the position of the reflected laser beam. b) SEM image of the cross-section of the Cr contacts/20GDC thin film on a $40 \text{ mm} \times 8 \text{ mm} \times 150 \mu\text{m}$ glass cantilever, used in ref. [74]. Similar measurements were made in ref. [57], using Ti contacts and (100) cut Si wafer as a substrate. Adapted with permission.^[74] Copyright 2016, Wiley-VCH.

$$\Delta k = \Delta X / (2 \cdot L \cdot l) \quad (9)$$

where Δk is the change in curvature, L is the distance from the sample to the CCD camera, and l is the distance on the sample between the reflection point to the clamping point (Figure 14). From the change in curvature, the change in stress in the films can be calculated by Stoney's formula^[75]

$$\Delta \sigma = \frac{Y_s}{(1 - \nu_s)} \frac{t_s^2}{6t_f} \Delta k \quad (10)$$

where Y_s is the Young's modulus of the substrate and ν_s is the Poisson ratio of the substrate, and t_s, t_f are the thicknesses of the substrate and film, respectively. For a 40 mm long cantilever, stress <10 MPa in a 100 nm thick film on 200 μm thick Si substrate is readily detected.

2. By measuring the change in curvature in different locations of the cantilever (i.e., scanning along the cantilever), one can verify whether the stress in the film is homogeneous. This is an advantage compared to techniques measuring average curvature (e.g., parallel beam^[76,77]) since inhomogeneity of curvature along the cantilever indicates inhomogeneity of stress and may confuse interpretation of the results.

Measurements of the electrostriction stress coefficient with this technique^[57,74] revealed that a few volts applied across a 0.5 μm thick film of $\text{Ce}_{1-x}\text{Gd}_x\text{O}_{2-x/2}$, $x = 0.1-0.33$ (20–60 kV cm^{-1} field), generated in-plane stress exceeding 100 MPa^[57] and, for some samples, reaching 500 MPa.^[74] From the direction of deflection of the cantilever, one could conclude that the films expanded in-plane, i.e., perpendicular to the applied field. However, it was not possible to detect whether the films contracted in the direction transverse to the field. Estimates of M_{xyy} from the data on the in-plane stress^[57] consistently yield values above $10^{-18} \text{ m}^2 \text{ V}^{-2}$ and for $\text{Ce}_{0.9}\text{Gd}_{0.1}\text{O}_{1.95}$ it is $M_{xyy} = 1.6 \times 10^{-17} \text{ m}^2 \text{ V}^{-2}$, which is orders of magnitude larger than predicted by Equation (8)^[59] ($70-120 \text{ m}^4 \text{ C}^{-2}$). The induced stress is proportional to the square of the electric field, as expected for electrostriction (Equation (4)), which also agrees with that the fact that application of the slowly alternating sinusoidal voltage (U_{AC}) results in second harmonic response. Superimposing a constant voltage, U_{DC} , with U_{AC} produces a mixture of first and second harmonics

$$\sigma \propto \left\{ U_{AC} \cdot \cos(2\pi ft) + U_{DC} \right\}^2 = U_{DC}^2 + \frac{U_{AC}^2}{2} + 2U_{AC} \cdot U_{DC} \cdot \cos(2\pi ft) + \frac{U_{AC}^2}{2} \cos(2 \cdot 2\pi ft) \quad (11)$$

In agreement with Equation (11), the amplitude of the stress response at the first harmonic was directly proportional to the product of U_{AC} and U_{DC} and the ratio of the stress response at the first and second harmonics was $4U_{DC}/U_{AC}$ (Figure 15a). Interestingly, films of undoped, but oxygen deficient, ceria also exhibit the electrostriction effect;^[57] however, annealing these films in oxygen leads to a considerable reduction of the electrostriction response. This supports the idea that the electrostriction effect in ceria requires the presence of oxygen vacancies. Nevertheless, the magnitude of the electrostrictive

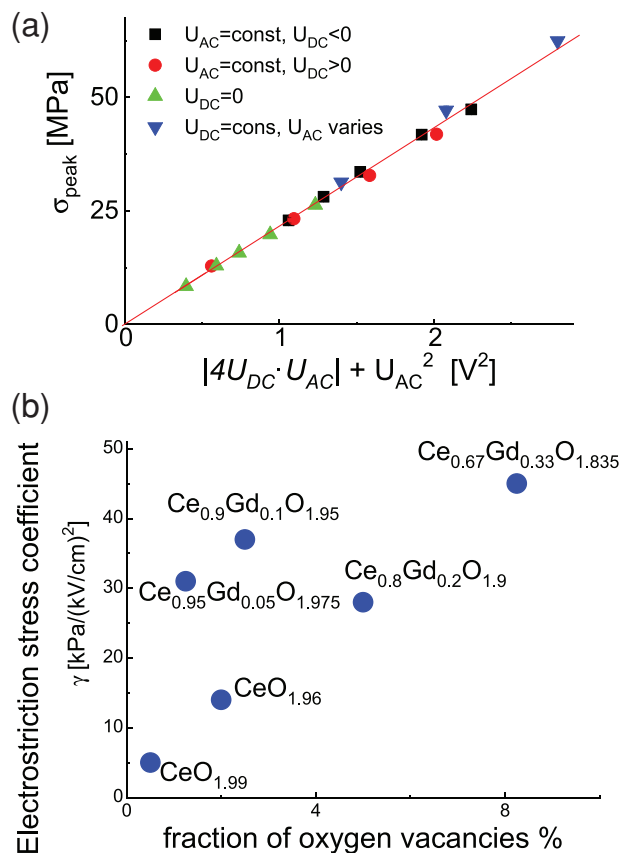


Figure 15. a) The peak values of in-plane electrostrictive stress developed in a 400 nm thick film of $\text{Ce}_{0.8}\text{Gd}_{0.2}\text{O}_{1.9}$ deposited on a glass cantilever with Cr electrodes as a function of applied voltages U_{DC} and U_{AC} . The frequency of U_{AC} was 10 mHz. The peak value of the stress is linearly proportional to the sum $4U_{DC} \cdot U_{AC} + U_{AC}^2$ (Equation (11)) with the first term measured at the first harmonic and the second term measured at the second harmonic. b) Dependence of the electrostriction stress-field coefficient γ on the concentration of oxygen vacancies for thin films of undoped and Gd-doped ceria. The film with 33 mol% Gd was in the fluorite phase according to X-ray diffraction (no double fluorite-related peaks were observed).^[74]

response of supported Gd-doped ceria films does not scale with the concentration of vacancies: rather, the dependence of the electrostriction strain coefficient on oxygen vacancy concentration appears to be more complex (Figure 15b). We note that X-ray diffraction measurements of a substrate-supported film with 33 mol% Gd did not show any indication of vacancy ordering,^[57] while powders of the same composition are in the double fluorite phase.^[16,46]

Observation of electrostriction in thin substrate-supported films by Lubomirsky and co-workers^[57,74,78] was recently confirmed by Murali and co-workers at Ecole Polytechnique Federale de Lausanne.^[79] Using a similar experimental arrangement, they found an electrostriction strain coefficient of $(9.0 \pm 0.5) \times 10^{-19} \text{ m}^2 \text{ V}^{-2}$. Interestingly, Hadad et al.^[79] were the first to point out that serious experimental difficulties derive from the quality and/or interface resistance of the electrical contacts. The authors compared Pt, Cr, and Al electrodes, noticing that hysteresis and differences in the magnitude of the

response can likely be traced to contact resistance. Moreover, the authors pointed out that the oxygen deficient and therefore more electrically conductive films apparently perform better, probably because they contain a higher concentration of vacancies as well as lower contact resistance. We also note that there is considerable difference in the range of frequencies used for the investigations in Korobko et al.^[57,74] and Hadad et al.^[79] The former used quasistatic electric fields, i.e., frequency of a few mHz, while Hadad et al.^[79] did not measure below 22 Hz.

3.3. Electrostriction in Self-Supported Films (Membranes) of Gd-Doped Ceria

Following the literature reports of electrostriction in substrate-supported $\text{Ce}_{0.8}\text{Gd}_{0.2}\text{O}_{1.9}$ films, two groups described electrostrictive behavior in self-supported $\text{Ce}_{0.8}\text{Gd}_{0.2}\text{O}_{1.9}$ films (membranes). The first report^[80] used 2 mm diameter, 1.4 μm thick films sandwiched between two Ti electrodes. When the film was released from the Si substrate, and clamped only at its circumference, the membranes remained flat at room temperature but buckled upon heating above 60 °C, indicating the presence of in-plane strain (tension). Displacement of the center of the membrane was measured with a modified Michelson interferometer stabilized by an external proportional-integral-derivative (PID) feedback system. The advantage of this approach is that the interferometer can measure the displacement of less than 1 nm; however, the lower frequency limit is 2 Hz due to the reaction time of the feedback loop.

The authors observed only second harmonic response to the applied voltage. Interpretation of the data was complicated by difficulty in separating the effects of thermo-electromechanical (Joule) heating from electrostriction. The amplitude of the out-of-plane deflection of the film under an electric field increased with increasing temperature. Relaxation of the membrane following step-like excitation could be described as exponential decay with time constant $\tau_{\text{st}} \approx 20$ ms (50 Hz), independent of temperature or amplitude of the applied bias (Figure 16a). The fact that the response is independent of temperature or amplitude of the applied bias raises the possibility that the response is produced by Joule heating (thermal expansion of the membrane). The response of a system to periodic heating with a well-defined thermal time constant is described by a first-order differential equation, the solution to which is well known. If such a membrane experiences sinusoidal heating with frequency $f = 1/\tau_{\text{st}}$, i.e., ≈ 50 Hz, the phase of the response should lag that of the excitation by $\approx \pi/2$ radians (viz. appendices in Lubomirsky and Stafsudd^[81]). When the driving frequency f is reduced to the single Hz range (in Figure 16b, i.e., much lower than $1/\tau_{\text{st}}$, the membrane response to Joule heating would be expected to follow the thermal excitation more closely and to be less dependent on frequency. For $f \ll 1/(10 \cdot \tau_{\text{st}})$, the expected phase lag is less than $2\pi/10$ radians. Since the phase shift of the membrane displacement as a function of excitation frequency that is actually observed (Figure 16b) is not consistent with the thermal model, then we must assume that Joule heating (thermal expansion) is not the only determining factor in the membrane displacement behavior. Ushakov et al.^[80] performed finite-element modeling using the COMSOL Multiphysics program with the MEMS

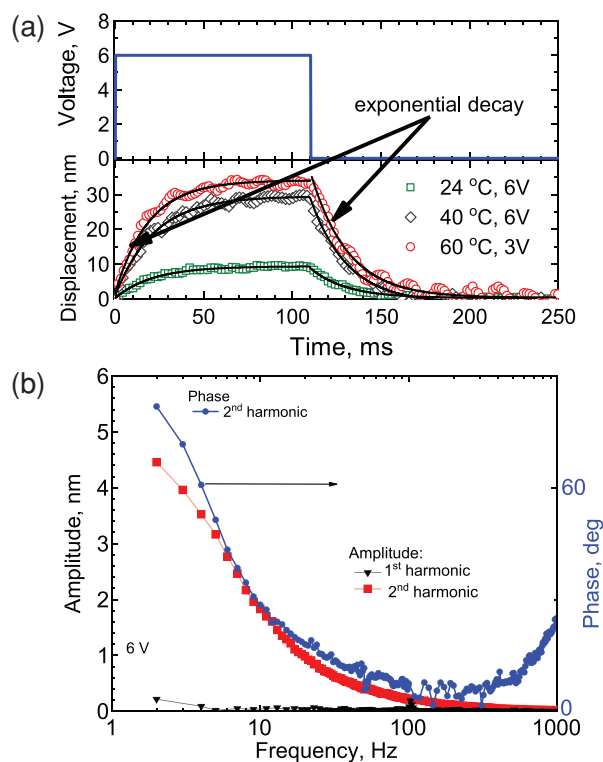


Figure 16. a) Electromechanical response of a 2 mm diameter, 1.4 μm thick 20GDC membrane with 150–200 nm thick Ti electrodes to a 6 V square pulse. The characteristic displacement relaxation time $\tau \approx 20$ ms and did not depend on the temperature or the applied bias. b) Amplitude of the displacement of the membrane as a function of the frequency of the applied voltage and the relative phase shift of the response. Adapted with permission.^[80] Copyright 2013, American Institute of Physics.

module to estimate the transverse electrostriction strain coefficient as $5 \times 10^{-18} \text{ m}^2 \text{ V}^{-2}$, which is close to the values reported by Korobko et al.^[57,74] for substrate-supported films.

Mishuk et al.^[7] used a different approach for characterizing the electromechanical response of ceria membranes. Their samples were 1–2 μm thick $\text{Ce}_{0.8}\text{Gd}_{0.2}\text{O}_{1.9}$ membranes, which buckled downward upon substrate removal, acquiring a soup-bowl shape. In addition, displacement was measured with an atomic force microscope tip with a built-in thermocouple to monitor temperature in situ. Application of 10 V peak-to-peak voltage at frequencies >100 kHz caused large (0.5 μm) vertical displacement of the membrane center. Under these conditions, the power dissipated in the membrane approaches a few tens of mW and the temperature at the center of the membrane increased ≈ 8 K above ambient. In this high-frequency mode, dominated by Joule heating, all membranes, irrespective of the contact metal, Al, Cr, Ni, or Ti, behaved similarly. From the thermal expansion coefficient of the components and the temperature distribution within a circular membrane clamped at the periphery,^[81] lattice strain was estimated. At low frequencies (0.5–10 Hz), membranes with Al, Ni, or Cr contacts did not demonstrate measurable electromechanical activity. Application of very high electric fields (30 V/1.5 μm) produced some response; however, this was usually accompanied by electrical breakdown. On the other hand, membranes with Ti contacts

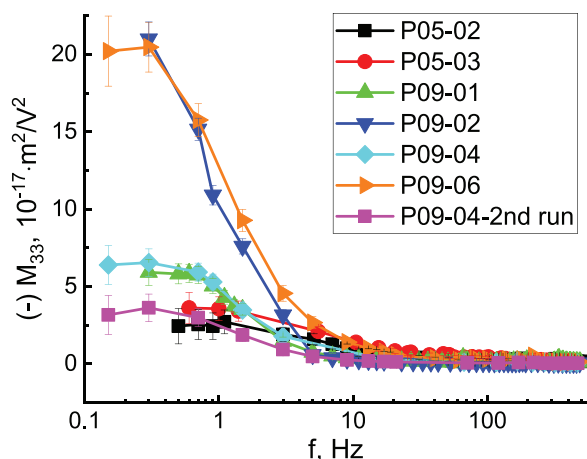


Figure 17. Frequency-dependent relaxation of the longitudinal electrostrictive strain coefficient M_{33} of six 10 mol% Gd-doped ceria pellets in AC electric fields of $<10 \text{ kV cm}^{-1}$ with frequency $f < 500 \text{ Hz}$. Below $\approx 5 \text{ Hz}$, there is a maximum of 1 order of magnitude spread in the values of M_{33} . Adapted with permission.^[72] Copyright 2018, Elsevier.

produced vertical displacement as large as 500 nm at 6 V. Displacement was linearly proportional to the applied voltage squared and was not accompanied by any detectable ($<0.1 \text{ K}$) heating, necessary evidence for electrostriction. Impedance spectroscopy data revealed that the lack of low-frequency electromechanical response of membranes with Al, Ni, or Cr electrodes was due to the contact resistance in the range of $\text{M}\Omega$ for 2 mm films. In the case of Ti, the measured resistance of the contacts decreased ≈ 3 orders of magnitude, which explains the observation of electromechanical response. Comparison of strain induced by Joule heating at higher frequencies with the strain induced by low-frequency electrostriction permits an estimate of the strain electrostriction coefficient as $4 \times 10^{-18} \text{ m}^2 \text{ V}^{-2}$, which is similar to the values for substrate-supported^[57,79] and self-supported films^[80] described above.

3.4. Electrostriction in Bulk $\text{Ce}_{0.9}\text{Gd}_{0.1}\text{O}_{1.95}$ Ceramics

With the aim of extending the characterization of electrostriction in Gd-doped ceria beyond thin films, Yavo et al.^[72] reported measurement of the electrostrictive strain coefficients in bulk $\text{Ce}_{0.9}\text{Gd}_{0.1}\text{O}_{1.95}$ ceramics. Since the comparison of the results of Korobko et al.^[57] and Hadad et al.^[79] revealed that the amplitude of the electrostrictive response in thin films appeared to decrease with increasing electric field frequency, Yavo et al.^[72] designed a system based on a capacitive proximity sensor.^[82] This sensor is capable of measuring mechanical displacement parallel to the applied field, which is accurate to within 0.05 nm and with frequencies ranging from a few tenths to a few hundred Hz. Yavo et al.^[72] reported that dense $\text{Ce}_{0.9}\text{Gd}_{0.1}\text{O}_{1.95}$ ceramics contracted in the direction of the electric field. This is consistent with the earlier finding that the thin films expand in the direction transverse to the electric field. All samples showed a non-ideal Debye-like relaxation with a characteristic relaxation time of 0.8–3 s. Above the relaxation frequency, the electrostriction strain coefficient was $|M_{33}^0| \approx 10^{-18} \text{ m}^2 \text{ V}^{-2}$, while below the relaxation frequency, the electrostriction strain coefficient displayed

large sample-to-sample variability $|M_{33}^0| \approx (2\text{--}20) \times 10^{-17} \text{ m}^2 \text{ V}^{-2}$ (Figure 17). The variability of the electrostriction coefficient did not correlate with the grain size or with the sample thickness. From impedance spectra acquired under different constant bias at various temperatures (25–150 °C), it was possible to conclude that the grain boundaries are blocking, which is expected for Gd-doped ceria ceramics.^[83–85] However, this work^[72] also showed that the grain boundaries are electronically conductive and trap charges under electric field. Therefore, they are most probably the cause of the spread in values of the electrostriction strain coefficient as well as the strain saturation with increasing electric field amplitude ($<2 \text{ ppm}$). On the one hand, these data fully confirm the phenomenon of nonclassical electrostriction in Gd-doped ceria, while on the other hand they point to a number of experimental challenges associated with both measuring and determining the origin of this effect.

3.5. Electromechanical Response of Gd-Doped Ceria at Room Temperature: Contact Resistance

We have shown that accurately assessing the value of the electrostriction strain coefficient in Gd-doped ceria thin films and ceramics at room temperature is experimentally difficult. One confounding element is the contact resistance, which may be present in the interface between the metal electrode and the ceria sample. The contact resistance can mask the true value of the electric field in the ceria grains. If the contacts are blocking for electronic current, then applying voltage may produce a space charge layer that screens the electric field inside the sample. The time necessary for the formation of such a layer at room temperature can be estimated from the value of the self-diffusion coefficient because it requires physical transfer of the oxygen vacancies into the space charge layer. However, though small ($\approx 10^{-19} \text{ cm}^2 \text{ s}^{-1}$ ^[86]) the diffusion coefficient and the corresponding ionic mobility will lead to the formation of a space charge layer within a few seconds. This constrains reliable measurement to frequencies above $\approx 10 \text{ mHz}$, which is indeed the lowest frequency used in Yavo et al.^[72] Moreover, for the case of blocking electrodes, $|M_{33}^0|$ may be overestimated because an inhomogeneous distribution of the electric field can produce displacement parallel to the field which is larger than in the case of a homogeneous field distribution. Indeed, the displacement δd is given by $M_{33}^0 \cdot (U/d)^2$, where U is the applied voltage and d is the thickness of the sample. For example, if the voltage is concentrated in only half of the sample thickness, then $\delta d = M_{33}^0 \cdot 4U^2/d$. This does not introduce ambiguity into measurement of thin films because the transverse electrostriction coefficient, M_{31}^0 , responds to the average field. However, if a ceramic sample is sufficiently thick, then the partitioning of the voltage will be such that the voltage drop on the body of the sample will always be larger than that at the contacts. Indeed, the typical specific resistivity of the grain interiors of $\text{Ce}_{0.9}\text{Gd}_{0.1}\text{O}_{1.95}$ ceramics used in Yavo et al.^[72] is a few $\text{G}\Omega$, which implies that the contact resistance is much smaller than that of the bulk. However, we note that thinning ceramic pellets, in an effort to increase the effective electric field under the same applied voltage, could again reduce the reliability of M_{33}^0 .

If the metal contacts are not blocking, then a chemical reaction may take place at the electrodes. For ceria, this presents

a problem related to the chemo-electromechanical effect:^[87] changes in composition are accompanied by changes in the unit cell volume. Chemomechanical effects are readily distinguished from electrostriction: the reduction of ceria causes lattice expansion while the oxidation of ceria causes lattice contraction or oxygen evolution when further cation oxidation is not possible. Consequently, chemomechanical effects are asymmetric with respect to the direction of the applied voltage and the sample will respond to the first harmonic of the frequency of the applied voltage. Therefore, the dominant electromechanical response reported in Yavo et al.^[72,82] for bulk ceramics of $\text{Ce}_{0.9}\text{Gd}_{0.1}\text{O}_{1.95}$ and (Nb,Y) stabilized δ -phase bismuth oxide was correctly identified: 1) it is symmetric with respect to the direction of the field (second harmonic) and 2) the sample contracts parallel to the direction of the field. From this point of view, measurements with ceramic samples are easier to interpret and validate than those made on thin films.

4. Concluding Remarks

4.1. Searching for an Atomic-Level Mechanism for Anelasticity and Electrostriction in Ceria

Characterizing the room-temperature anelastic and electromechanical properties of doped and reduced ceria and determining their structural origins is obviously a work in progress. Although the near neighbor environments of both host and dopant cations in the ceria lattice have been a subject of investigation by synchrotron X-ray diffraction, X-ray absorption spectroscopy, and neutron diffraction, a detailed understanding of the anomalous behavior of oxygen deficient ceria will require additional measurements of elastic moduli and electromechanical activity under varying conditions of dopant chemistry, temperature, strain, geometry, and electrode metal. Generally, modeling of solid electrolytes, such as ceria, has concentrated on explaining the diffusion coefficients of the oxygen ions and oxidation/reduction kinetics with much less emphasis on mechanical properties. Indeed, no simulation capable of empirically reproducing the unrelaxed elastic moduli has been presented to date. Even when compared to other anelastic materials containing point-defect induced elastic dipoles, ceria is exceptional: the difference between the relaxed and unrelaxed biaxial moduli of 20 mol% Gd-doped ceria is unusually large (approx. a factor of 10); the magnitude of the strain associated with anelastic relaxation (0.1–0.4%) as well as the large range of relaxation times has not been observed elsewhere.

4.2. A Few Suggestions for Specific Mechanical and Electromechanical Measurements to Provide Additional Modeling Constraints

i) *Chemistry*: Comparing the mechanical behavior of thin film and bulk ceria ceramics with aliovalent dopants other than Gd, for which measurements are available in the literature; providing such measurements when the necessary data for comparisons are not currently available. Answering questions such as: to what extent does crystallite (grain) size and preferential

orientation in thin films influence anelastic behavior? Do lattice defects produced by either the dopant cations or that of the oxygen vacancies dominate the mechanical behavior?

- ii) *Geometry*: Developing a technique to measure the longitudinal and transverse electrostrictive strain coefficients M_{33} and M_{31} on the same sample, preferably with the same instrumentation, so that changes in the unit cell volume during electrostriction could be reliably determined. This would require the preparation of large grain, dense ceramic samples, for which the influence of the electrode contacts and grain boundaries would not be significant.
- iii) *Temperature dependence*: Conduct a wide spectrum (mHz to Hz) dynamic mechanical analysis measuring internal friction as a function of temperature (–100 to +200 °C) and load. Internal friction measurements may provide answers regarding the activation energy associated with the rearrangement of the elastic dipole strain fields responsible for the anelasticity. We note, however, that such measurements would require the preparation of ceramic samples with a high aspect ratio (typically >15:1).

4.3. Significance for Practical Device Design and Engineering

In-depth understanding of the mechanical anomalies in Gd-doped ceria will ultimately influence design of practical, thin film-based MEMS devices. From the above, it is clear that the preparation of such devices must contend with at least two types of problems.

- i) Anelastic effects control time-dependent strain and, thereby, also the shape and surface area of self-supported membrane structures. Since anelastic strain may reach 0.4%, films of doped ceria have a strong tendency to buckle upon substrate release.^[6,21,22,34] The extent of the buckling, which may be expected to occur, is defined by the degree of strain relaxation during preparation, but also by device operating temperature. MEMS engineers will have to find a way to minimize this problem.
- ii) Assuming that a MEMS device containing a reduced or doped ceria thin film is successfully built, there still remains the possibility that the application of a few volts of external bias at an operating temperature for which the electrostriction effect is significant would generate hundreds of MPa in-plane stress, compromising mechanical integrity. Since electrostriction cannot be eliminated, one solution would be to design the device in such a way that subsequent expansion/contraction of the structure due to electrostriction could be accommodated. This problem, however, is a detail of mechanical engineering and not intended for consideration in the context of the current review.

Acknowledgements

I.L. and A.I.F. acknowledge the National Science Foundation–US-Israeli Binational Science foundation (NSF-BSF) program supported under Grant No. 2015679. A.I.F. acknowledges support by the NSF under Grant No. DMR-1701747. This work was supported in part by the Israeli Ministry of Science and Technology under Grant No. 3-12944. This research was made possible in part by the historic generosity of the Harold Perlman Family.

Conflict of Interest

The authors declare no conflict of interest.

Keywords

anelasticity, creep, Gd-doped ceria, nonclassical electrostriction, Young's modulus

Received: December 21, 2017

Revised: March 5, 2018

Published online: July 8, 2018

- [1] H. Inaba, H. Tagawa, *Solid State Ionics* **1996**, *83*, 1.
- [2] C. Chatzichristodoulou, P. T. Blennow, M. Søgaard, P. V. Hendriksen, M. B. Mogensen, in *Catalysis by Ceria and Related Materials*, 2nd ed., Catalytic Science Series, Vol. 12, (Ed.: A. Trovarelli), Imperial College Press, London, UK **2013**, p. 623.
- [3] M. Mogensen, N. M. Sammes, G. A. Tompsett, *Solid State Ionics* **2000**, *129*, 63.
- [4] L. Vivier, D. Duprez, *Chemsuschem* **2010**, *3*, 654.
- [5] R. J. Gorte, *AIChE J.* **2010**, *56*, 1126.
- [6] Y. N. Shi, I. Garbayo, P. Murali, J. L. M. Rupp, *J. Mater. Chem. A* **2017**, *5*, 3900.
- [7] E. Mishuk, E. Makagon, E. Wachtel, S. R. Cohen, R. Popovitz-Biro, I. Lubomirsky, *Sens. Actuators, A* **2017**, *264*, 333.
- [8] E. Wachtel, I. Lubomirsky, *Scr. Mater.* **2011**, *65*, 112.
- [9] N. Yavo, D. Noiman, E. Wachtel, S. Kim, Y. Feldman, I. Lubomirsky, O. Yeheskel, *Scr. Mater.* **2016**, *123*, 86.
- [10] R. Korobko, S. K. Kim, S. Kim, S. R. Cohen, E. Wachtel, I. Lubomirsky, *Adv. Funct. Mater.* **2013**, *23*, 6076.
- [11] R. Korobko, C. T. Chen, S. Kim, S. R. Cohen, E. Wachtel, N. Yavo, I. Lubomirsky, *Scr. Mater.* **2012**, *66*, 155.
- [12] A. S. Nowick, B. S. Berry, *Anelastic Relaxation in Crystalline Solids*, Academic Press, New York **1972**.
- [13] M. Ricken, J. Nolting, I. Riess, *J. Solid State Chem.* **1984**, *54*, 89.
- [14] S. Hull, S. T. Norberg, I. Ahmed, S. G. Eriksson, D. Marrocchelli, P. A. Madden, *J. Solid State Chem.* **2009**, *182*, 2815.
- [15] L. P. Li, J. C. Nino, *J. Eur. Ceram. Soc.* **2012**, *32*, 3543.
- [16] A. Kossoy, Q. Wang, R. Korobko, V. Grover, Y. Feldman, E. Wachtel, A. K. Tyagi, A. I. Frenkel, I. Lubomirsky, *Phys. Rev. B* **2013**, *87*, 1.
- [17] L. P. Li, R. Kasse, S. Phadke, W. Qiu, A. Huq, J. C. Nino, *Solid State Ionics* **2012**, *221*, 15.
- [18] G. Mazzolai, *AIP Adv.* **2011**, *1*.
- [19] H. Numakura, M. Koiwa, *J. Phys. IV* **1996**, *6*, 97.
- [20] J. C. Qiao, J. M. Pelletier, *J. Mater. Sci. Technol.* **2014**, *30*, 523.
- [21] A. Kossoy, Y. Feldman, R. Korobko, E. Wachtel, I. Lubomirsky, J. Maier, *Adv. Funct. Mater.* **2009**, *19*, 634.
- [22] A. Kossoy, Y. Feldman, E. Wachtel, I. Lubomirsky, J. Maier, *Adv. Funct. Mater.* **2007**, *17*, 2393.
- [23] A. Kossoy, A. I. Frenkel, Y. Feldman, E. Wachtel, A. Milner, I. Lubomirsky, *Solid State Ionics* **2010**, *181*, 1473.
- [24] R. Gerhardt, F. Zamaninoor, A. S. Nowick, C. R. A. Catlow, A. N. Cormack, *Solid State Ionics* **1983**, *9–10*, 931.
- [25] R. Gerhardt, W. K. Lee, A. S. Nowick, *J. Phys. Chem. Solids* **1987**, *48*, 563.
- [26] K. W. Lay, D. H. Whitmore, *Phys. Status Solidi B* **1971**, *43*, 175.
- [27] O. Kraynis, E. Wachtel, I. Lubomirsky, T. Livneh, *Scr. Mater.* **2017**, *137*, 123.
- [28] A. Atkinson, A. Selcuk, *Solid State Ionics* **2000**, *134*, 59.
- [29] R. Maurya, A. Gupta, S. Omar, K. Balani, *Ceram. Int.* **2016**, *42*, 11393.
- [30] H. X. Xu, R. K. Behera, Y. L. Wang, F. Ebrahimi, S. B. Sinnott, E. D. Wachsman, S. R. Phillpot, *Solid State Ionics* **2010**, *181*, 551.
- [31] K. L. Duncan, Y. L. Wang, S. R. Bishop, F. Ebrahimi, E. D. Wachsman, *J. Appl. Phys.* **2007**, *101*, 044906.
- [32] K. L. Duncan, Y. L. Wang, S. R. Bishop, F. Ebrahimi, E. D. Wachsman, *J. Am. Ceram. Soc.* **2006**, *89*, 3162.
- [33] A. Kossoy, A. I. Frenkel, Q. Wang, E. Wachtel, I. Lubomirsky, *Adv. Mater.* **2010**, *22*, 1659.
- [34] Y. U. Shi, A. H. Bork, S. Schweiger, J. L. M. Rupp, *Nat. Mater.* **2015**, *14*, 721.
- [35] W. W. Gerberich, M. J. Cordill, *Rep. Prog. Phys.* **2006**, *69*, 2157.
- [36] V. Grover, A. K. Tyagi, *Mater. Res. Bull.* **2004**, *39*, 859.
- [37] T. S. Zhang, P. Hing, H. T. Huang, J. Kilner, *Solid State Ionics* **2002**, *148*, 567.
- [38] F. Y. Wang, B. Z. Wan, S. F. Cheng, *J. Solid State Electrochem.* **2005**, *9*, 168.
- [39] I. Mahata, G. Das, R. K. Mishra, B. P. Sharma, *J. Alloys Compd.* **2005**, *391*, 129.
- [40] G. Brauer, H. Gradinger, *Z. Anorg. Allg. Chem.* **1954**, *276*, 209.
- [41] A. Kossoy, H. Cohen, T. Bendikov, E. Wachtel, I. Lubomirsky, *Solid State Ionics* **2011**, *194*, 1.
- [42] A. Kossoy, E. Wachtel, I. Lubomirsky, *J. Electroceram.* **2014**, *32*, 47.
- [43] N. Goykhman, Y. Feldman, E. Wachtel, A. Yoffe, I. Lubomirsky, *J. Electroceram.* **2014**, *33*, 180.
- [44] G. N. Greaves, A. L. Greer, R. S. Lakes, T. Rouxel, *Nat. Mater.* **2011**, *10*, 823.
- [45] J. R. McBride, K. C. Hass, B. D. Poindexter, W. H. Weber, *J. Appl. Phys.* **1994**, *76*, 2435.
- [46] C. Artini, M. Pani, M. M. Carnasciali, M. T. Buscaglia, J. R. Plaisier, G. A. Costa, *Inorg. Chem.* **2015**, *54*, 4126.
- [47] V. V. Sal'nikov, E. Y. Pikalova, *Phys. Solid State* **2015**, *57*, 1944.
- [48] G. A. Kourouklis, A. Jayaraman, G. P. Espinosa, *Phys. Rev. B* **1988**, *37*, 4250.
- [49] Y. Z. Shi, K. H. Stone, Z. X. Guan, M. Monti, C. T. Cao, F. El Gabaly, W. C. Chueh, M. F. Toney, *Phys. Rev. B* **2016**, *94*, 205420.
- [50] F. Iguchi, S. Onodera, N. Sata, H. Yugami, *Solid State Ionics* **2012**, *225*, 99.
- [51] Y. L. Wang, K. Duncan, E. D. Wachsman, F. Ebrahimi, *Solid State Ionics* **2007**, *178*, 53.
- [52] M. Morales, J. J. Roa, X. G. Capdevila, M. Segarra, S. Pinol, *Acta Mater.* **2010**, *58*, 2504.
- [53] J. G. Swallow, J. J. Kim, M. Kabir, J. F. Smith, H. L. Tuller, S. R. Bishop, K. J. Van Vliet, *Acta Mater.* **2016**, *105*, 16.
- [54] J. G. Swallow, J. J. Kim, S. R. Bishop, J. F. Smith, H. L. Tuller, K. J. Van Vliet, *ECS Trans.* **2015**, *68*, 847.
- [55] F. Ye, T. Mori, D. R. Ou, J. Zou, G. Auchterlonie, J. Drennan, *Solid State Ionics* **2008**, *179*, 827.
- [56] S. Swaroop, M. Kilo, A. E. Kossoy, I. Lubomirsky, I. Riess, *Solid State Ionics* **2008**, *179*, 1205.
- [57] R. Korobko, A. Lerner, Y. Y. Li, E. Wachtel, A. I. Frenkel, I. Lubomirsky, *Appl. Phys. Lett.* **2015**, *106*, 042904.
- [58] R. D. Shannon, *Acta Crystallogr. A* **1976**, *32*, 751.
- [59] R. E. Newnham, V. Sundar, R. Yimnirun, J. Su, Q. M. Zhang, *J. Phys. Chem. B* **1997**, *101*, 10141.
- [60] TRS Technologies, Electrostrictors, <http://www.trstechnologies.com/Materials/Electrostrictive-Ceramics>, (accessed: May 2018).
- [61] D. S. Fu, H. Taniguchi, M. Itoh, S. Koshihara, N. Yamamoto, S. Mori, *Phys. Rev. Lett.* **2009**, *103*, 207601.
- [62] S. Nomura, K. Tonooka, J. Kuwata, L. E. Cross, R. E. Newnham, *Ferroelectrics* **1980**, *29*, 124.
- [63] L. Bohaty, S. Haussuhl, *Acta Crystallogr., Sect. A: Cryst. Phys., Diffraction, Theor. Gen. Crystallogr.* **1977**, *33*, 114.
- [64] Q. M. Zhang, V. Bharti, X. Zhao, *Science* **1998**, *280*, 2101.
- [65] Q. Chen, K. Ren, B. Chu, Y. Liu, Q. M. Zhang, V. Bobnar, A. Levstik, *Ferroelectrics* **2007**, *354*, 178.

- [66] R. Pirc, R. Blinc, V. Bobnar, A. Gregorovic, *Ferroelectrics* **2007**, 347, 7.
- [67] N. Uchida, T. Ikeda, *Jpn. J. Appl. Phys.* **1967**, 6, 1079.
- [68] Z. Y. Meng, U. Kumar, L. E. Cross, *J. Am. Ceram. Soc.* **1985**, 68, 459.
- [69] A. Kholkin, C. Tantigate, A. Safari, *Integr. Ferroelectr.* **1998**, 22, 1035.
- [70] F. Li, L. Jin, Z. Xu, S. J. Zhang, *Appl. Phys. Rev.* **2014**, 1, 011103.
- [71] V. Shelukhin, I. Zon, E. Wachtel, Y. Feldman, I. Lubomirsky, *Solid State Ionics* **2012**, 211, 12.
- [72] N. Yavo, O. Yeheskel, E. Wachtel, D. Ehre, A. I. Frenkel, I. Lubomirsky, *Acta Mater.* **2018**, 144, 411.
- [73] K. Uchino, *J. Phys. Soc. Jpn.* **1984**, 53, 1531.
- [74] R. Korobko, A. Patlolla, A. Kossoy, E. Wachtel, H. L. Tuller, A. I. Frenkel, I. Lubomirsky, *Adv. Mater.* **2012**, 24, 5857.
- [75] G. G. Stoney, *Proc. R. Soc. London, Ser. A* **1909**, 82, 172.
- [76] A description of the parallel beam approach can be found at <https://www.k-space.com/>.
- [77] B. W. Sheldon, V. B. Shenoy, *Phys. Rev. Lett.* **2011**, 106, 216104.
- [78] R. Korobko, E. Wachtel, I. Lubomirsky, *Sens. Actuators, A* **2013**, 201, 73.
- [79] M. Hadad, H. Ashraf, G. Mohanty, C. Sandu, P. Murali, *Acta Mater.* **2016**, 118, 1.
- [80] A. D. Ushakov, E. Mishuk, E. Makagon, D. O. Alikin, A. A. Esin, I. S. Baturin, A. Tselev, V. Y. Shur, I. Lubomirsky, A. L. Kholkin, *Appl. Phys. Lett.* **2017**, 110, 142902.
- [81] I. Lubomirsky, O. Stafsudd, *Rev. Sci. Instrum.* **2012**, 83, 1.
- [82] N. Yavo, A. D. Smith, O. Yeheskel, S. R. Cohen, R. Korobko, E. Wachtel, P. R. Slater, I. Lubomirsky, *Adv. Funct. Mater.* **2016**, 26, 1138.
- [83] S. Kim, J. Fleig, J. Maier, *Phys. Chem. Chem. Phys.* **2003**, 5, 2268.
- [84] H. J. Avila-Paredes, S. Kim, *Solid State Ionics* **2006**, 177, 3075.
- [85] H. J. Avila-Paredes, K. Choi, C. T. Chen, S. Kim, *J. Mater. Chem.* **2009**, 19, 4837.
- [86] P. S. Manning, J. D. Sirman, R. A. DeSouza, J. A. Kilner, *Solid State Ionics* **1997**, 100, 1.
- [87] J. G. Swallow, J. J. Kim, J. M. Maloney, D. Chen, J. F. Smith, S. R. Bishop, H. L. Tuller, K. J. Van Vliet, *Nat. Mater.* **2017**, 16, 749.
- [88] U. Hennings, R. Reimert, *Appl. Catal. A* **2007**, 325, 41.